SANDIA REPORT

SAND2014-20708
Unlimited Release
Printed December 2014

Mechanical Characterization of Rigid Polyurethane Foams

Wei-Yang Lu

Prepared by
Sandia National Laboratories
Albuquerque, New Mexico 87185 and Livermore, California 94550

Sandia National Laboratories is a multi-program laboratory managed and operated by Sandia Corporation, a wholly owned subsidiary of Lockheed Martin Corporation, for the U.S. Department of Energy's National Nuclear Security Administration under contract DE-AC04-94AL85000.

Issued by Sandia National Laboratories, operated for the United States Department of Energy by Sandia Corporation.

Available to DOE and DOE contractors from
U.S. Department of Energy
Office of Scientific and Technical Information
P.O. Box 62
Oak Ridge, TN 37831

Telephone: (865) 576-8401
Facsimile: (865) 576-5728
E-Mail: reports@adonis.osti.gov
Online ordering: http://www.osti.gov/bridge

Available to the public from
U.S. Department of Commerce
National Technical Information Service
5285 Port Royal Rd.
Springfield, VA 22161

Telephone: (800) 553-6847
Facsimile: (703) 605-6900
E-Mail: orders@ntis.fedworld.gov
Online order: http://www.ntis.gov/help/ordermethods.asp?loc=7-4-0#online

SAND2014-20708
Unlimited Release
Printed December 2014

Mechanical Characterization of Rigid Polyurethane Foams

Wei-Yang Lu
Mechanics of Materials
Sandia National Laboratories
P.O. Box 5800
Albuquerque, New Mexico 87185-MSXXXX

Abstract

Foam materials are used to protect sensitive components from impact loading. In order to predict and simulate the foam performance under various loading conditions, a validated foam model is needed and the mechanical properties of foams need to be characterized.

Uniaxial compression and tension tests were conducted for different densities of foams under various temperatures and loading rates. Crush stress, tensile strength, and elastic modulus were obtained. A newly developed confined compression experiment provided data for investigating the foam flow direction. A biaxial tension experiment was also developed to explore the damage surface of a rigid polyurethane foam.

ACKNOWLEDGMENTS

Thank Mike Neilsen, Terry Hinnerichs, David Lo, Helena Jin, Bo Song, and Professor Weinong Chen for technical discussions, John Korellis and Pat Keifer for suggesting and design experimental method, Simon Scheffel, Simon Lee and Edwin Huestis for running part of the experiments, and David Epp and Chris O'Gorman for program support.

CONTENTS

FIGURES

TABLES

NOMENCLATURE

UCPD	Unified Creep Plasticity Damage model
PMDI	Polymethylene Diisocyanate
pcf	pound per cubic foot
KCP	Kansas City Plant
AR	Aspect ratio
DIC	digital image correlation
TEMA	track eye motion analysis software
kip	kilopound

1. INTRODUCTION

This report documents the experiments and results that characterize mechanical behaviors of rigid polyurethane foams and support the development of constitutive models for these materials. They are used to absorb energy during impact events by undergoing large deformation. Unified Creep Plasticity Damage (UCPD) model [1, 2] is being developed at Sandia to describe foam response to large deformation at various loading conditions. As the name of the model indicates, it describes foam's plasticity-like crush behavior, rate (or time) dependent behavior, and damage and failure. A validated model is needed in finite element analyses to simulate impact events of foam components in application.

1.1. Materials

The foams of interest here are PMDI (Polymethylene Diisocyanate) and TufFoam foams of various densities. For PMDI foams, this study includes five nominal densities: 10, 20, 30, 40, and 50 pcf (pound per cubic foot). (Usually, the foam type and density are put together without the unit just for easily identifying the material. For example, PMDI10 means PMDI foams with a nominal density of 10 pcf.) All PMDI foams were produced by Kansas City Plant (KCP). Only two densities of TufFoam are included: 35 and 65 pcf. One batch of TufFoam35 was received from KCP; the second batch of TufFoam35 and TufFoam65 were manufactured by the Polymer Laboratory of Materials Chemistry Department, Sandia/California.

1.2. Experiments

Mechanical behaviors such as the temperature and rate effects of stress-strain curves, the pressure versus volume relation, the yield and damage surfaces, and the flow rule of plastic strain rate are critical parts of the model. A set of key experiments, described in the following, are necessary to calibrate and validate the model.

1.2.1. Uniaxial Compression

Uniaxial compression is the most common test, which provides basic stress-strain relation of the material, elastic modulus, yield stress, etc. Most available data are from tests conducted at quasi-static rate and room temperature. For the compression test included in this study, the temperature of interest covers a range from -65 to 180 ^{o}F; and the loading strain rate spans from 10^{-4} (quasi-static) to 10^{2} s^{-1}. Uniaxial compressions alone will not be sufficient to characterize the foam behavior. More experiments are required.

1.2.2. Rigid Confined Compression

Hydrostatic compression [3] is the preferred experiment to obtain the foam's pressure versus volume relation directly; however, performing the test has been very challenging. The specimen needs to be coated for the test. Preparing the coating is very tedious and the successful rate of the experiment is low. The issue is the integrity of the coating; it often leaks, especially for high density foams at high pressure. An alternative method is the rigid confined compression, where the foam is only allowed to deform in the loading direction but the deformation is suppressed in

lateral directions by rigid wall. The foam is subjected to tri-axial compression. Combining such results with the uniaxial compression data and the flow rule, the pressure-volume relation can be estimated. Unfortunately, the flow rule has not been identified by experiments as well. Different experiments need to be considered.

1.2.3. Elastic Confined Compression

A new confined compression test has been developed during this investigation. A thin wall tube, mounted with strain gages, is used to confine the foam deformation. The tube is designed so it experiences only elastic deformation during the test. Compressing foam sample inside the tube along its axis, both the lateral deformation of the foam and the pressure distribution inside the tube can be calculated from the hoop strain of the tube measured by strain gages. The axial force and displacement plus hoop strain data provide sufficient information about foam plastic flow. To draw the information from data, however, is complex. There is no simple equation that can convert the data to model parameters directly. It is usually done by numerical simulation.

1.2.4. Uniaxial Tensile Test

Foam's tensile behavior is different from compression. It is not very ductile and does not absorb much energy. The stress-strain relation in tension including failure stress is needed. In many applications some portion of a foam component is subject to tensile stress. The tensile behavior will affect the overall performance of a component.

1.2.5. Multi-axial Tensile Test

Also, during application the applied stress is hardly uniaxial. To construct the damage (or failure) surface of the model, multi-axial tensile tension data are needed. Little experiments are available in this area. A biaxial experiment is developed by considering combined tension and internal pressuring a foam tube.

2. UNIAXIAL COMPRESSION

2.1. Experimental methods

The experimental setup was based on a MTS servo-hydraulic system. As shown in Fig. 1(a), the test frame is coupled with an environmental chamber, and a specimen is mounted between two platens, magnified in Fig. 1(b). Cylindrical specimens were machine-cut out of foam blocks with dimensions were nominally one inch in diameter and height. Typically, a thin layer of Corning vacuum grease was applied at both ends of foam specimen to reduce friction. The test is run under displacement control. The actuator of the servo-hydraulic test frame compressed specimens to approximately 65% of its original height at the desired rate. When conducting elevated or cold temperature test, heated or chilled specimens were held at constant temperature in the environmental chamber for about one hour to allow the specimens to equilibrate with the chamber's temperature before loading.

Laser extensometer was used to measure displacement with reflective tape bonded to platens. For elevated or cold temperature test, the laser light was accessed through the chamber window. Force was measured by a load cell, which was outside the chamber at the ambient condition. In Fig. 1(a), it is located between the crosshead and the chamber.

The experimental results are presented in the following sections. Engineering stress versus engineering strain is displayed. Several issues related to foam compression test are addressed: temperature effect in section 2.2.2; strain rate effect in sections 2.2.2 and 2.2.6.2; density effect in section 2.3; specimen aspect ratio and lubrication in sections 2.2.2.1 and 2.2.4.1; unloading-reloading in sections 2.2.6.1 and 2.2.7; different batch of material in section 2.2.6.2, etc.

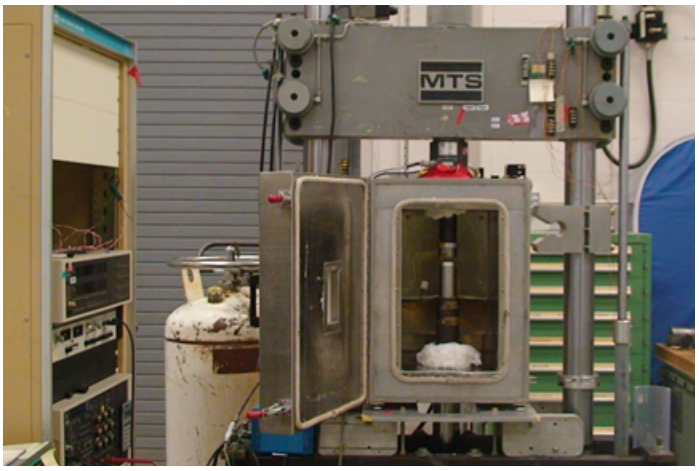

(a)

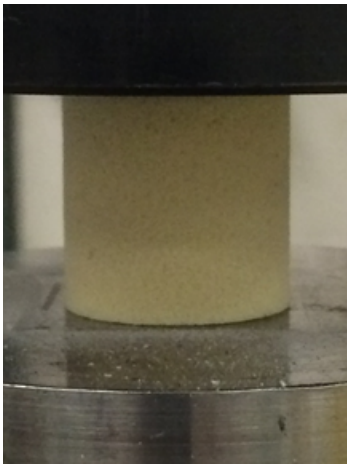

(b)

Figure 1 Foam compression experimental setup, (a) MTS High Rate system and environmental chamber, (b) foam compression specimen between platens.

2.2. Experimental results

The results are organized according to the foam material. Since the experiments were conducted over several years, some variations in test conditions exist among foams. PMDI20 has the most completed experimental conditions.

2.2.1. PMDI10

The results are organized according to the temperature conditions. Only one strain rate 0.01 per second was considered. Specimens and conditions are listed in Table 1 and engineering stress-strain curves are plotted in Fig. 2.

The stress-strain curves typically have a nearly constant stress region, which is the crush region, then stress increases again called lockup. The cold temperature curves, Fig. 2(c), are different from the others. Specimens were failed, broken into pieces, before the stress leveled. Comparing to the room temperature data, the PMDI10 yield (or crush) stress is lower more than 20% at 165^{o}F.

The density is also affect the yield stress, higher density specimen shows a higher yield stress, for example, A1 curve in Fig. 2(a).

2.2.2. PMDI20

PMDI20 has the most completed experimental data set. Four strain rates (0.0001, 0.01, 1.0 and 100 /s) were considered for three temperatures (70, -65, and 165 ^{o}F). Each case had at least three repeats. The detail test matrix is Table 2.

Engineering stress-strain curves are shown in Figs. 3-5. At 70 ^{o}F, only the 100/s samples failed before reaching plateau, Fig. 3(d). As strain approached 0.1, the stress dropped, which indicated specimen failure. At low temperature -65 ^{o}F, the foam failed at different regions depending on the loading rate: as shown in Fig. 4, at lockup when the loading is quasi-static (0.0001/s), at plateau when the loading is 0.01/s, and before plateau when the loading is 1.0/s or greater. At high temperature 165 ^{o}F, the only failure occurred was the fastest loading 100/s but it happened at the plateau, Fig 5(d).

The temperature and rate effects are summarized in Fig. 6. The crush stresses of those specimens displayed a plateau are plotted. For the temperature and rate ranges under consideration, the variation of crush stress and failure strain of foam could be very large.

Table 1 Test matrix of uniaxial compression of 10 pcf PMDI foam

Specimen	Diameter (in.)	Height (in.)	Density (pcf)	Temperature (degree F)	Rate (s^{-1})
A1	1.255	1.978	9.80	70	0.01
A2	1.257	0.970	9.73	70	0.01
A3	1.257	0.962	9.72	70	0.01
A4	1.257	0.954	9.71	-65	0.01
B2	1.255	1.005	9.84	165	0.01
B3	1.254	1.004	9.86	165	0.01
B4	1.255	0.999	9.80	165	0.01

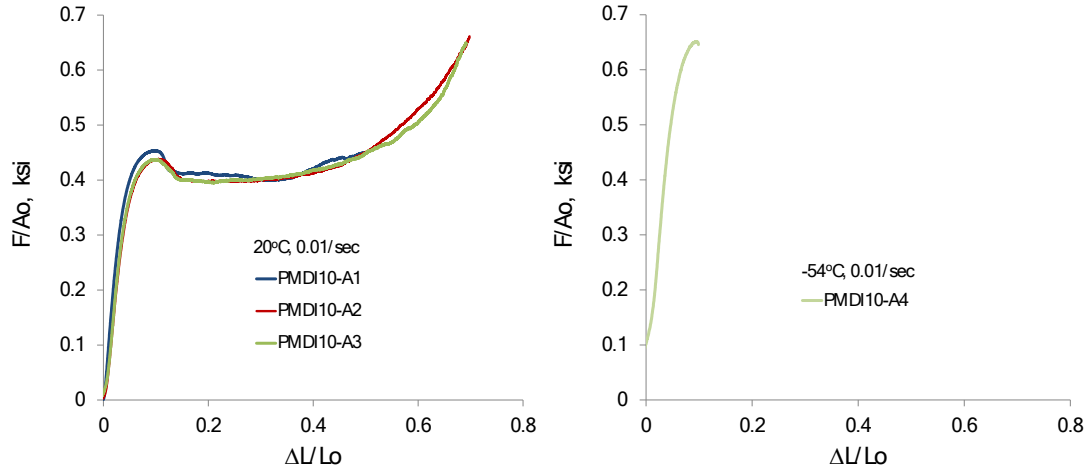

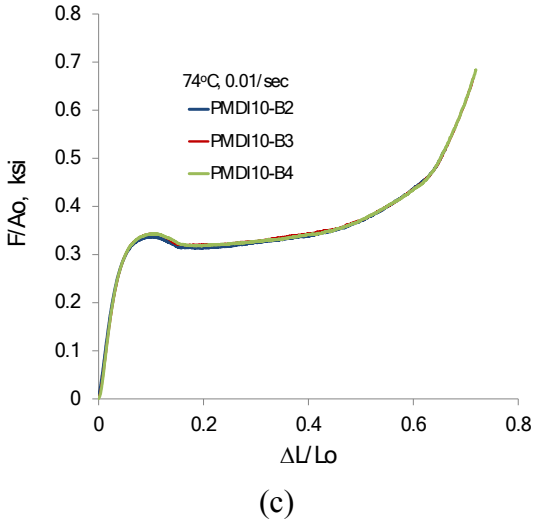

Figure 2 Stress-stress relations of PMDI10 at (a) 70°F, (b) -65°F, and (c) 165°F.

Table 2 Test matrix of uniaxial compression of 20 pcf PMDI foam

Specimen	Diameter (in.)	Height (in.)	Density (pcf)	Temp. (degree F)	Rate (s^{-1})
A24	1.030	0.995	18.08	70	E-04
A25	1.030	0.998	17.57		
A26	1.030	0.999	17.69		
A1	1.030	1.050	17.00	70	E-02
A2	1.035	1.000	18.12		
A3	1.038	1.050	17.03		
A27	1.030	0.999	17.65	70	E-00
A28	1.030	0.992	17.83		
A29	1.030	0.992	17.84		
B24	1.040	0.999	17.57	70	E02
B10	1.038	1.000	17.90		
B11	1.040	1.000	17.62		
B25	1.026	0.500	18.44		
B26	1.031	0.501	18.13		
A11	1.027	1.000	17.94	-65	E-04
B1	1.038	0.999	17.78		
B2	1.039	1.000	18.14		
A4	1.040	1.020	17.49	-65	E-02
A5	1.035	1.000	17.82		
A6	1.002	1.020	17.53		
B3	1.040	1.004	18.17	-65	E-00
B4	1.038	1.000	18.25		
B5	1.036	0.998	18.23		
B6	1.039	1.004	17.74	-65	E02
B7	1.040	0.996	18.13		
B8	1.040	1.002	18.23		
B12	1.037	0.998	17.85	165	E-04
B13	1.038	0.998	18.21		
B14	1.037	1.000	17.97		
B15	1.039	1.000	17.76	165	E-02
B16	1.037	1.001	18.22		
B17	1.038	1.005	18.18		
B18	1.038	1.003	18.21	165	E-00
B19	1.039	1.000	17.66		
B20	1.038	1.003	17.84		
B21	1.038	1.003	17.68	165	E02
B22	1.038	1.003	17.78		
B23	1.035	1.004	18.10		

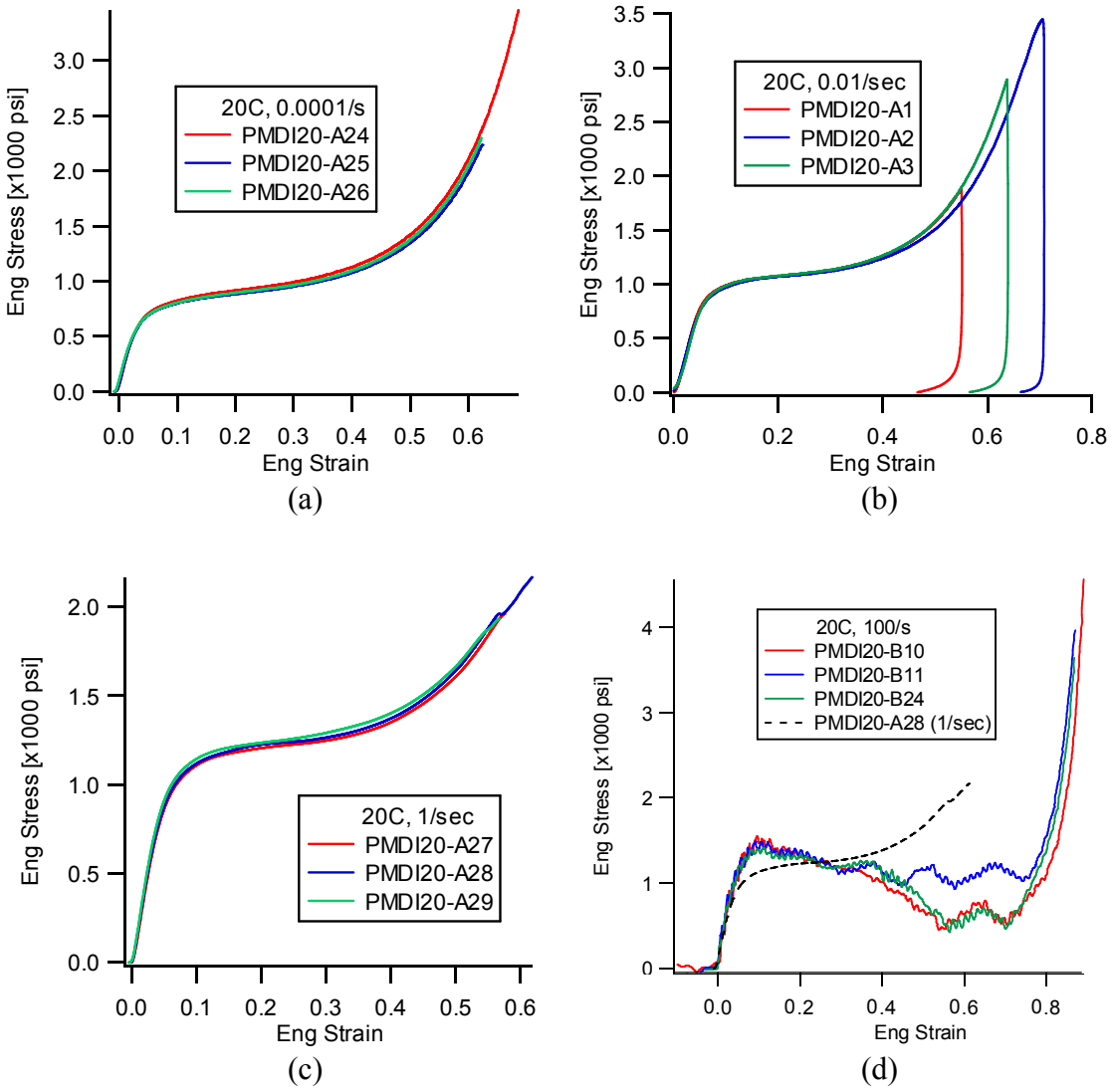

Figure 3 Engineering stress-stress relations of PMDI20 at 70°F for various strain rates (a) 0.0001/s, (b) 0.01/s, (c) 1.0/s, and (d) 100/s.

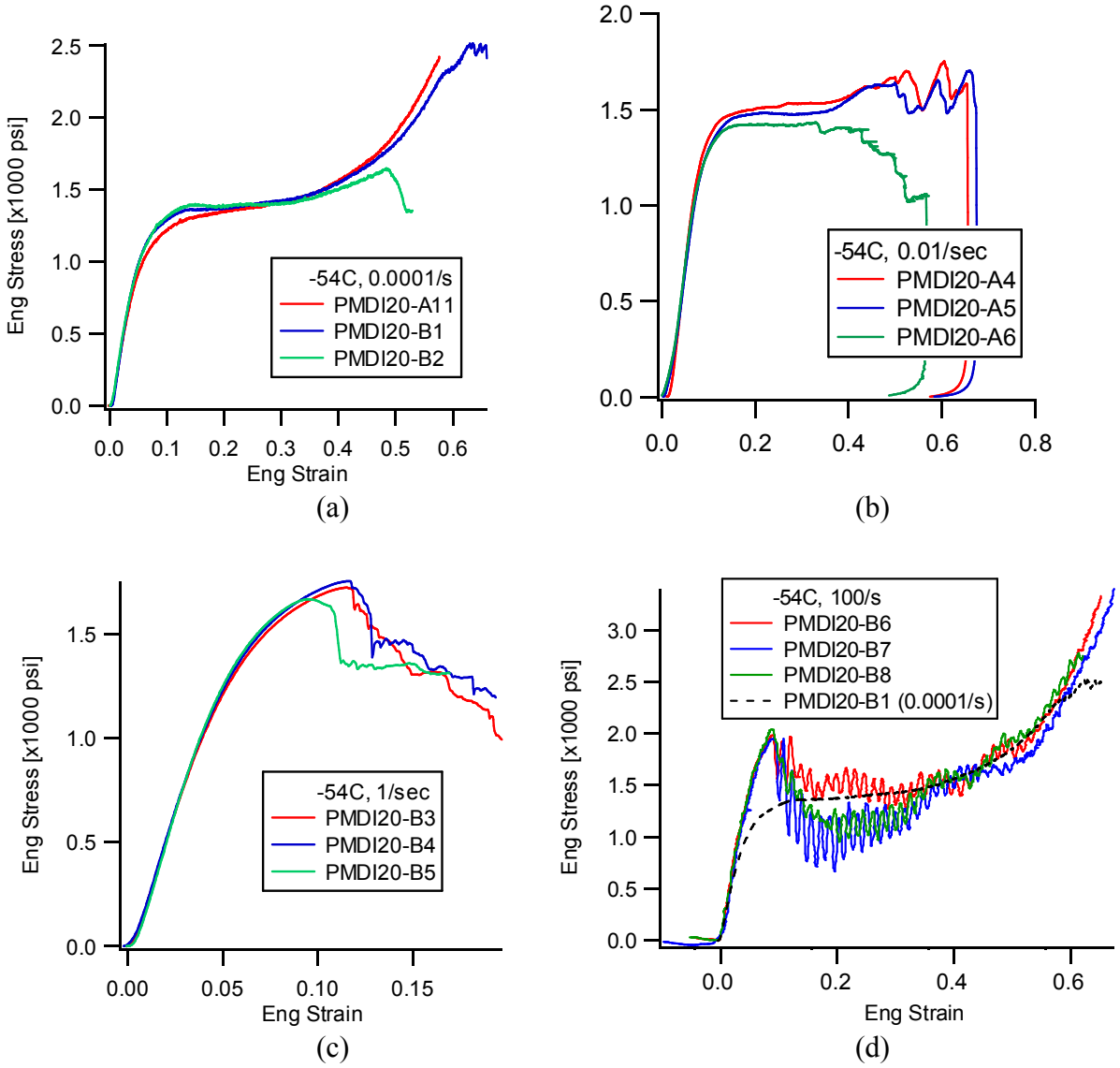

Figure 4 Engineering stress-stress relations of PMDI20 at -65°F for various strain rates (a) 0.0001/s, (b) 0.01/s, (c) 1.0/s, and (d) 100/s.

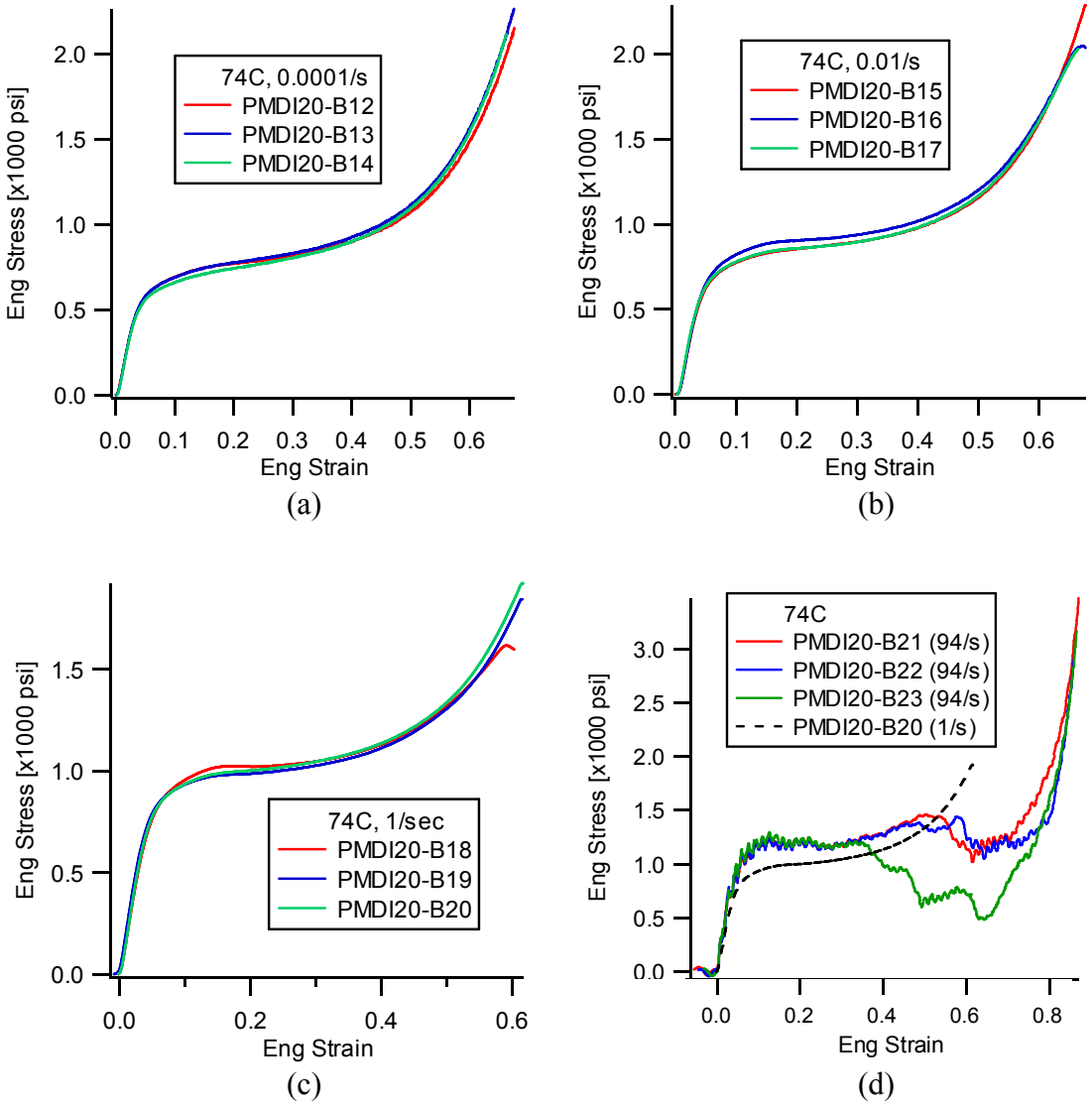

Figure 5 Engineering stress-stress relations of PMDI20 at 165°F for various strain rates (a) 0.0001/s, (b) 0.01/s, (c) 1.0/s, and (d) 100/s.

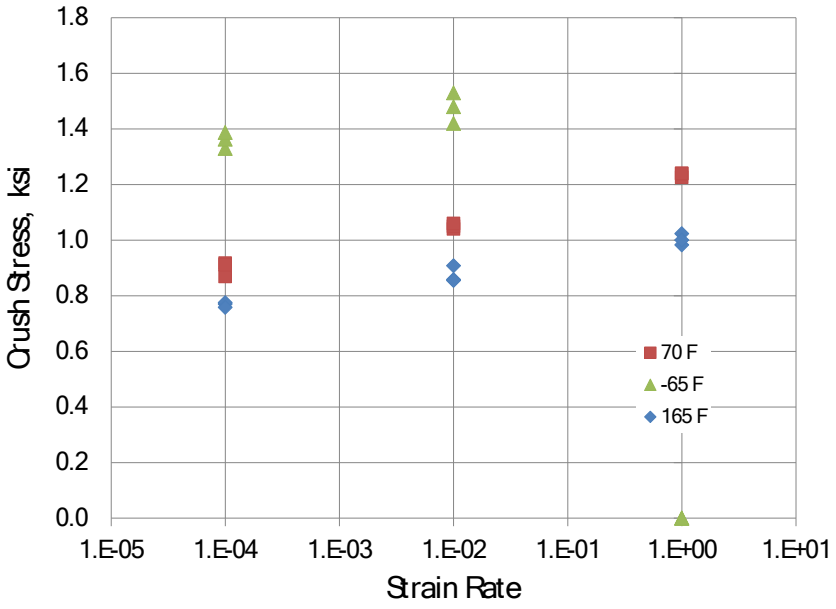

(a)

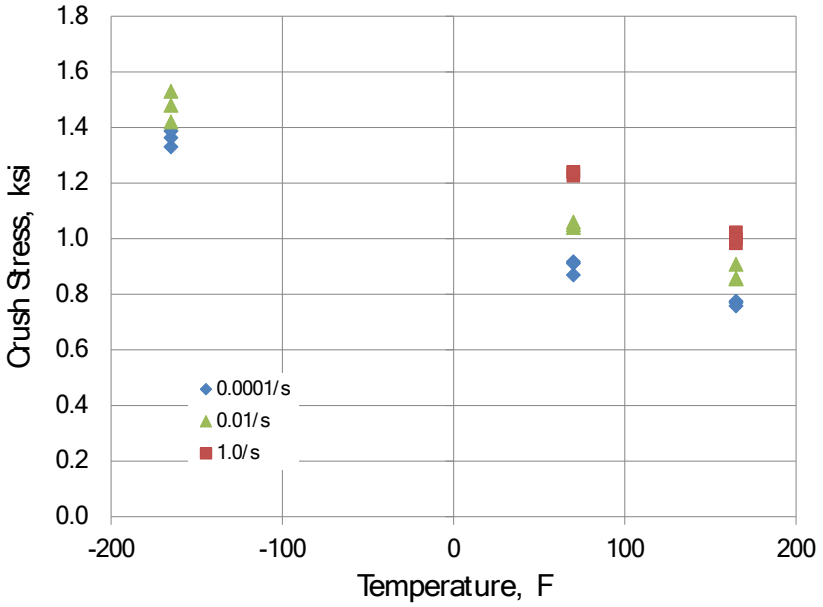

(b)

Figure 6 (a) Temperature and (b) rate effects on the crush stress of PMDI20.

2.2.2.1. Effects of Lubricant and Specimen Aspect Ratio

For an ideal compression test, the friction between specimen and platen is controlled so the specimen deformed uniformly without bulging; however, it has been difficult to achieve for a foam compression. Even with a thin layer of grease, foam specimens are bulging during compression, which indicates the friction at the interface preventing the foam deform radially. If there is a bulging, that means the foam is not deformed uniformly.

Since the test is less than ideal, specimen geometry may have some influences on the experimental result. The following set of tests is designed to study the effects of lubricant and specimen aspect ratio on the stress-strain response of foams. Additional PMDI20 specimens were utilized, Table 3.

All tests involved in this study had the same strain rate 0.01/s. Only with and without lubricant were considered. Aspect ratio (AR) is defined as AR = height / diameter; three different sample geometries were tested.

Keeping the temperature, strain rate, and aspect ratio constant, but by changing the lubricating conditions, the stress-strain curves are compared, shown in Fig. 7. Specimens A1-A5 have been listed in Table 2. There is little difference between lubricated and unlubricated specimens for tests at room temperature, Fig. 7(a) and (b), and low temperature -65^{o}F, Fig. 7(c).

Specimens with various aspect ratios show the same stress-strain curves. The results suggest that the effects of lubricant and aspect ratio on the stress-strain behavior can be neglected.

Table 3 Additional 20 pcf PMDI foam specimens

Specimen	Diameter (in.)	Height (in.)	Density (pcf)	Temperature (degree F)	Rate (s^{-1})	Lubricant	Aspect Ratio
A7	1.025	1.001	18.22	20	0.01	No	1.0
A8	1.025	1.000	17.86	20	0.01	No	1.0
A9	1.025	0.997	17.99	-54	0.01	No	1.0
A10	1.025	0.992	18.27	-54	0.01	No	1.0
A12	0.835	0.995	17.86	20	0.01	Yes	1.2
A13	0.835	1.003	18.16	20	0.01	Yes	1.2
A14	0.837	0.999	18.23	20	0.01	No	1.2
A15	0.840	1.000	18.12	20	0.01	No	1.2
A18	0.627	0.998	17.90	20	0.01	Yes	1.6
A19	0.628	0.998	17.97	20	0.01	Yes	1.6

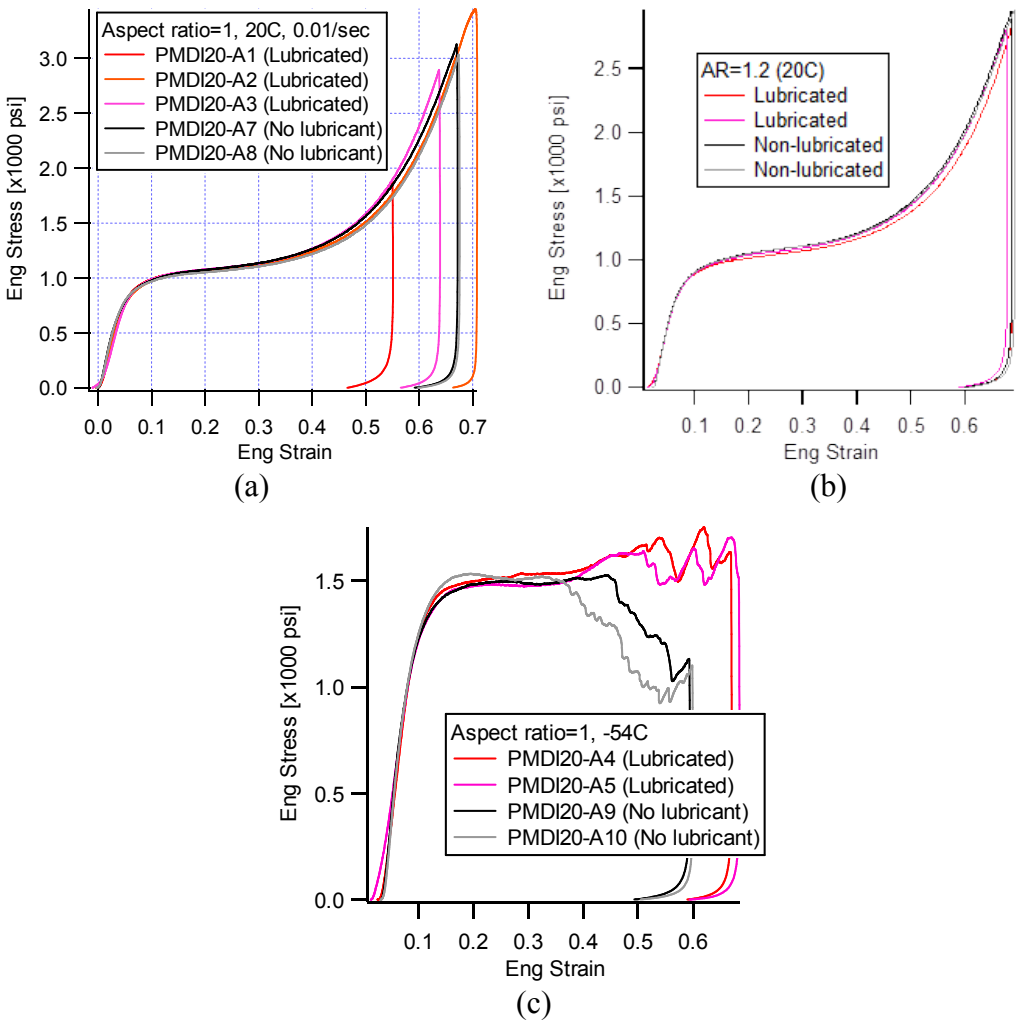

Figure 7 Effects of lubricant at: (a) 70°F, AR=1; (b) 70°F, AR=2; (c) -65°F, AR=1.

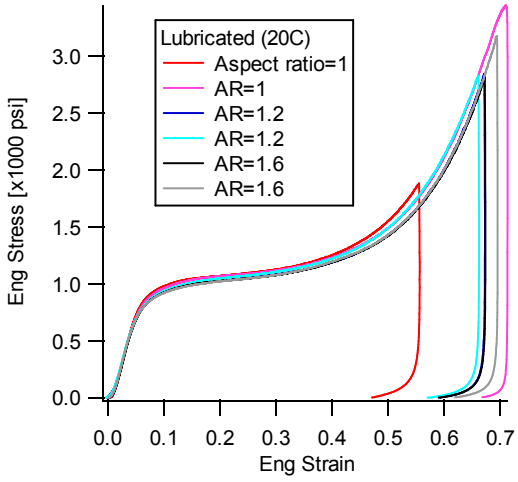

Figure 8 Effects of specimen aspect ratio.

2.2.3. PMDI30

Table 4 Test matrix of uniaxial compression of 30 pcf PMDI foam

Specimen	Diameter (in.)	Height (in.)	Density (pcf)	Temperature (degree F)	Rate (s^{-1})
A7	0.842	1.004	27.24	70	0.0001
A8	0.842	1.002	26.84		
A9	0.842	1.000	26.64		
A1	0.835	1.000	27.08	70	0.01
A2	0.835	0.998	28.83		
A3	0.835	1.000	28.46		
A10	0.842	1.002	26.82	70	1.0
A11	0.842	1.000	26.87		
A12	0.842	1.002	27.59		
A13	0.842	1.001	27.32	70	0.01
A14	0.843	0.996	26.63		
A15	0.843	1.003	26.86		
A4	0.835	0.997	29.12	-65	0.0001
A5	0.835	0.998	28.89		
A6	0.835	0.996	27.41		
A16	0.843	1.003	26.72	-65	0.01
A17	0.843	1.003	26.76		
A18	0.842	0.994	26.90		
A19	0.842	1.005	26.71	-65	1.0
A20	0.844	0.996	25.98		
A21	0.842	0.995	26.91		
A22	0.843	1.003	26.98	-65	0.01
A23	0.844	1.002	26.93		
A24	0.842	1.005	27.03		
A25	0.842	1.000	27.50	165	0.0001
A26	0.843	0.995	26.41		
A27	0.842	1.000	26.30		
A28	0.842	1.003	26.60	165	0.01
A29	0.842	0.993	26.67		
A30	0.843	1.004	28.23		
A31	0.843	1.002	28.47	165	1.0
A32	0.843	1.001	26.50		
A33	0.843	0.990	26.18		
B2	0.843	1.001	25.64	165	0.01
B3	0.842	1.003	25.67		
B4	0.842	0.999	25.68		

Similar to PMDI20, a set of compression experiments covered several orders of strain rate and a wide temperature range for PMDI30 was conducted. Notice the diameter of the specimen was 0.842 inch and the aspect ratio was about 1.2. The test matrix is in Table 4 and the results of 70°F, -65°F, and 165°F are plotted in Figs. 9, 10, and 11, respectively.

For the same test condition PMDI30 fails at a smaller strain than PMDI20. At room temperature, it failed in the plateau region at strain rate 0.01/s, Fig. 9(b). At low temperature -65°F, it failed before the plateau region even at quasi-static rate, Fig. 10(a). The data are consistent with general trends observed from PMDI10 and PMDI20. Small difference in density can result in noticeable changes in the stress-strain curve. For example, specimen A25 in Fig. 10(a), A30 in Fig. 10(b), or A31 in Fig. 10(c), its crush stresses is higher than the rest of the group.

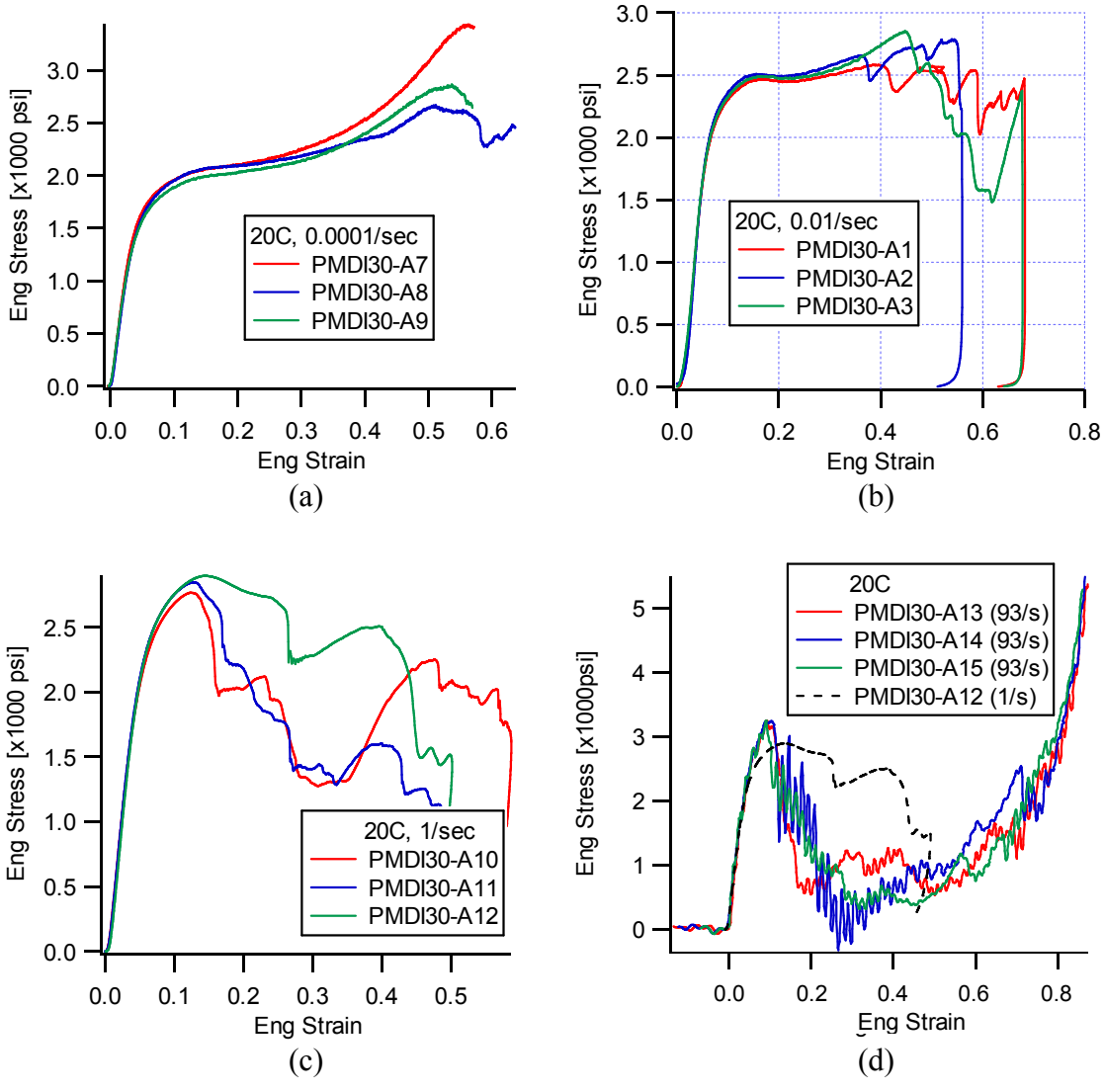

Figure 9 Engineering stress-stress relations of PMDI30 at 70°F for various strain rates (a) 0.0001/s, (b) 0.01/s, (c) 1.0/s, and (d) 100/s.

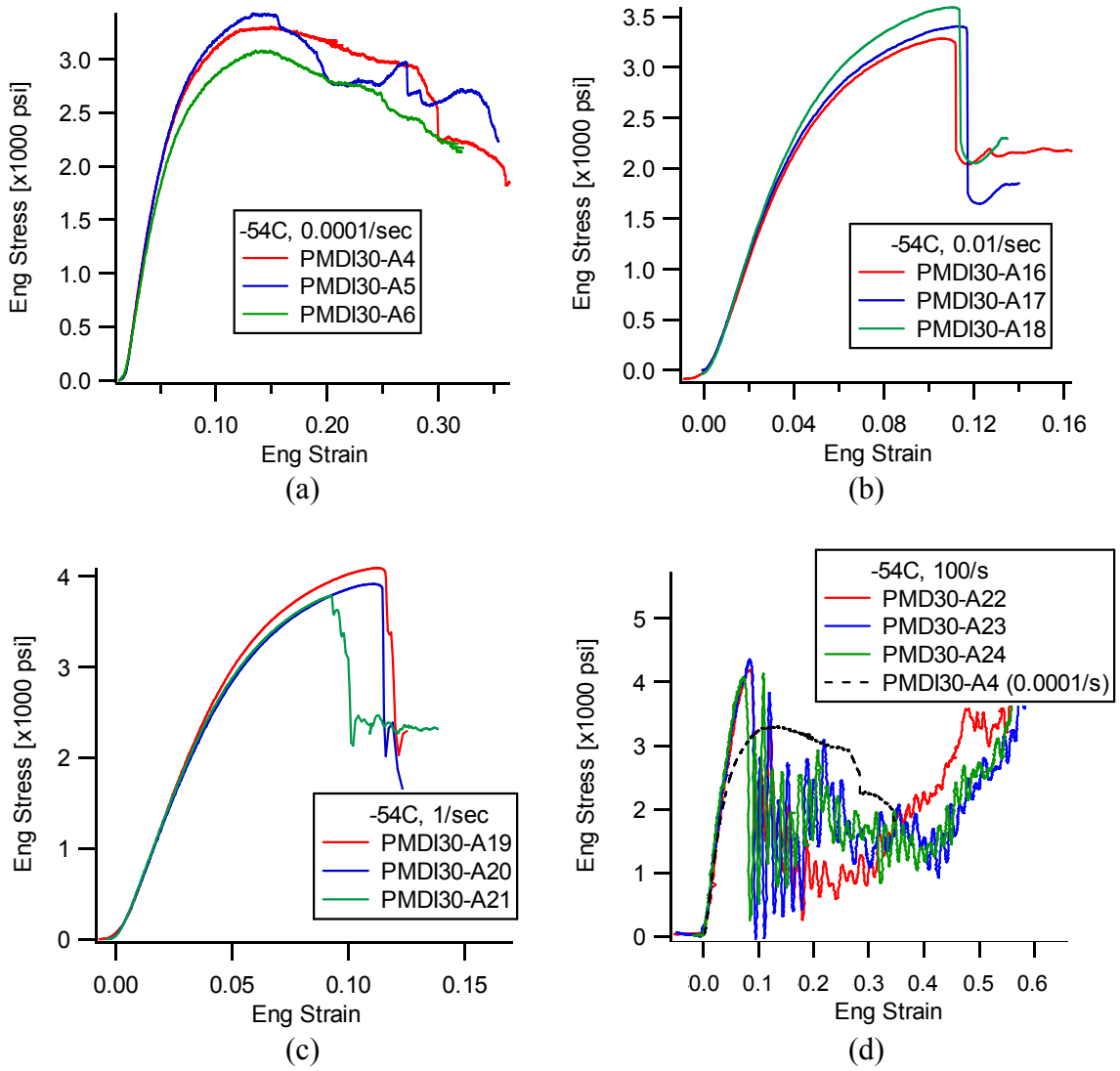

Figure 10 Engineering stress-stress relations of PMDI30 at -65°F for various strain rates (a) 0.0001/s, (b) 0.01/s, (c) 1.0/s, and (d) 100/s.

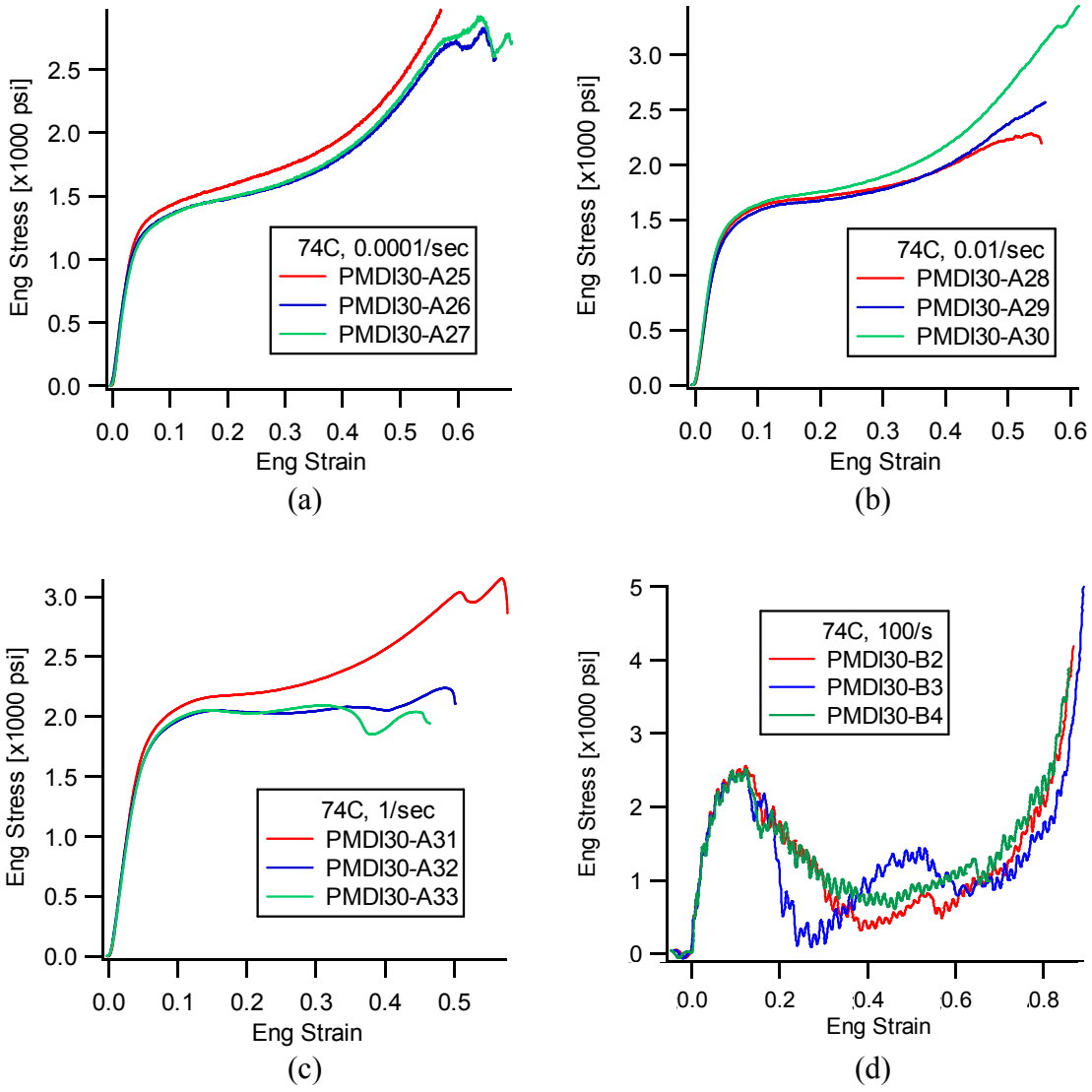

Figure 11 Engineering stress-stress relations of PMDI30 at 165°F for various strain rates (a) 0.0001/s, (b) 0.01/s, (c) 1.0/s, and (d) 100/s.

2.2.4. PMDI40

Table 5 Test matrix of uniaxial compression of 40 pcf PMDI foam

Specimen	Diameter (in.)	Height (in.)	Density (pcf)	Temperature (degree F)	Rate (s^{-1})
A21	0.635	1.000	34.50	70	0.0001
A22	0.632	1.000	34.78		
A23	0.628	1.001	34.47		
A1	0.628	0.998	34.20	70	0.01
A2	0.628	1.002	34.43		
A3	0.629	1.000	34.12		
A24	0.636	0.999	34.27	70	1.0
A25	0.633	1.003	34.27		
A26	0.634	0.993	33.89		
A27	0.633	1.002	33.92	70	100
A28	0.635	1.000	34.03		
A29	0.635	0.999	34.23		
A30	0.635	1.002	33.93	-165	0.0001
A31	0.638	1.000	33.95		
A32	0.637	1.002	34.38		
A33	0.638	0.998	34.91	-165	0.01
A34	0.632	1.003	34.73		
A35	0.630	0.995	34.40		
A36	0.632	1.000	34.73	-165	1.0
A37	0.632	0.997	35.09		
A38	0.629	1.004	34.41		
A39	0.630	0.997	34.69	-165	100
A40	0.634	1.002	35.55		
A41	0.632	1.018	34.45		
A42	0.633	1.002	34.07	165	0.0001
A43	0.624	1.003	34.46		
A44	0.632	1.005	34.42		
A45	0.629	1.002	34.06	165	0.01
A46	0.632	0.999	34.47		
A47	0.632	1.004	34.65		
A48	0.631	0.998	34.53	165	1.0
A49	0.633	0.935	34.69		
A50	0.628	0.999	34.83		
B1	0.632	1.000	34.67	165	100
B2	0.628	1.003	34.68		
B3	0.631	1.007	34.09		

The test matrix of PMDI40, Table 5, is similar to PMDI20 and PMDI30. The diameter of the specimen was 0.632 inch and the aspect ratio was about 1.6. Results are displayed in Figs. 12-14. At room temperature and high temperature, the failure strain of PMDI40 is smaller than PMDI30.

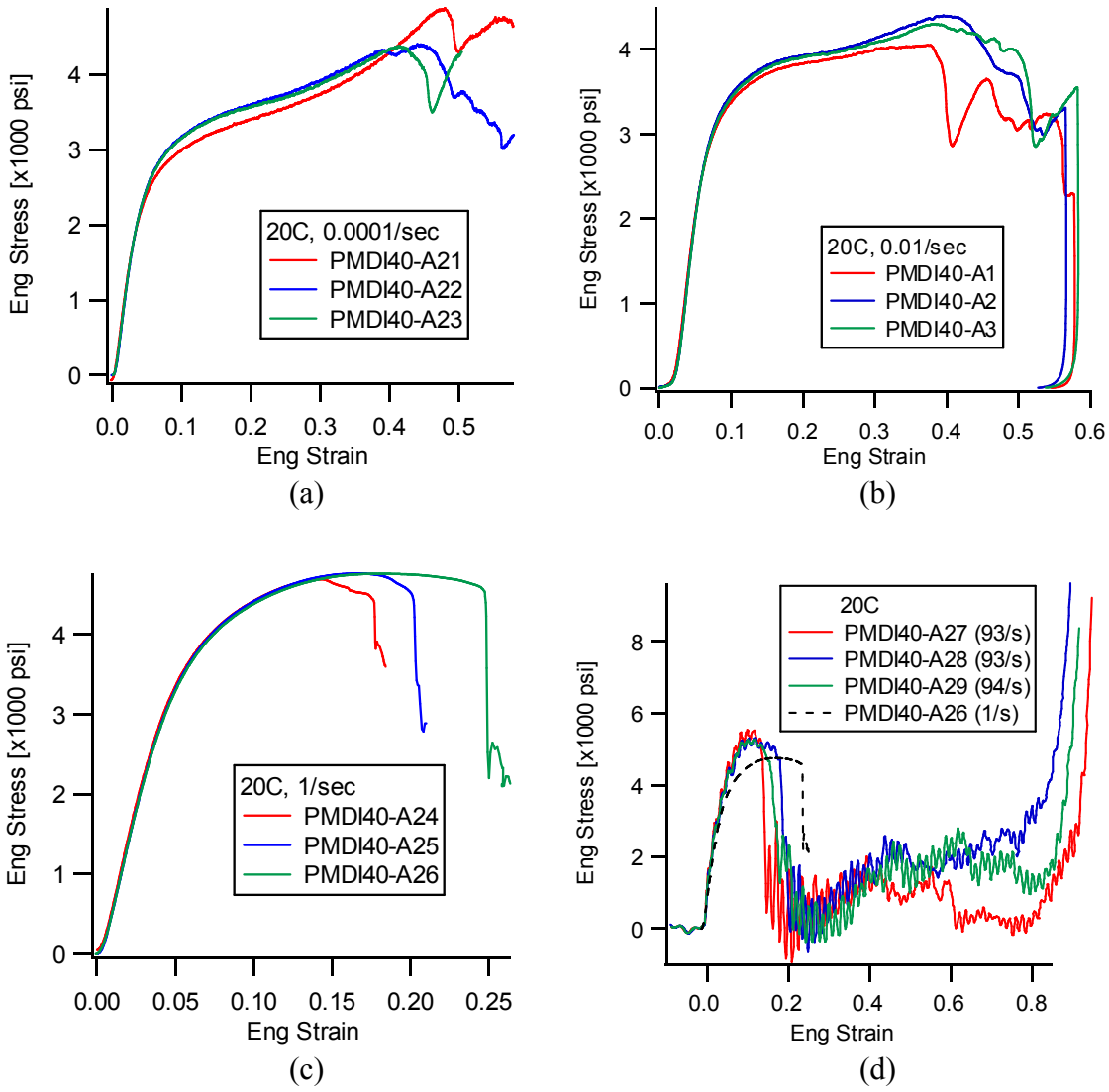

Figure 12 Engineering stress-stress relations of PMDI40 at 70°F for various strain rates (a) 0.0001/s, (b) 0.01/s, (c) 1.0/s, and (d) 100/s.

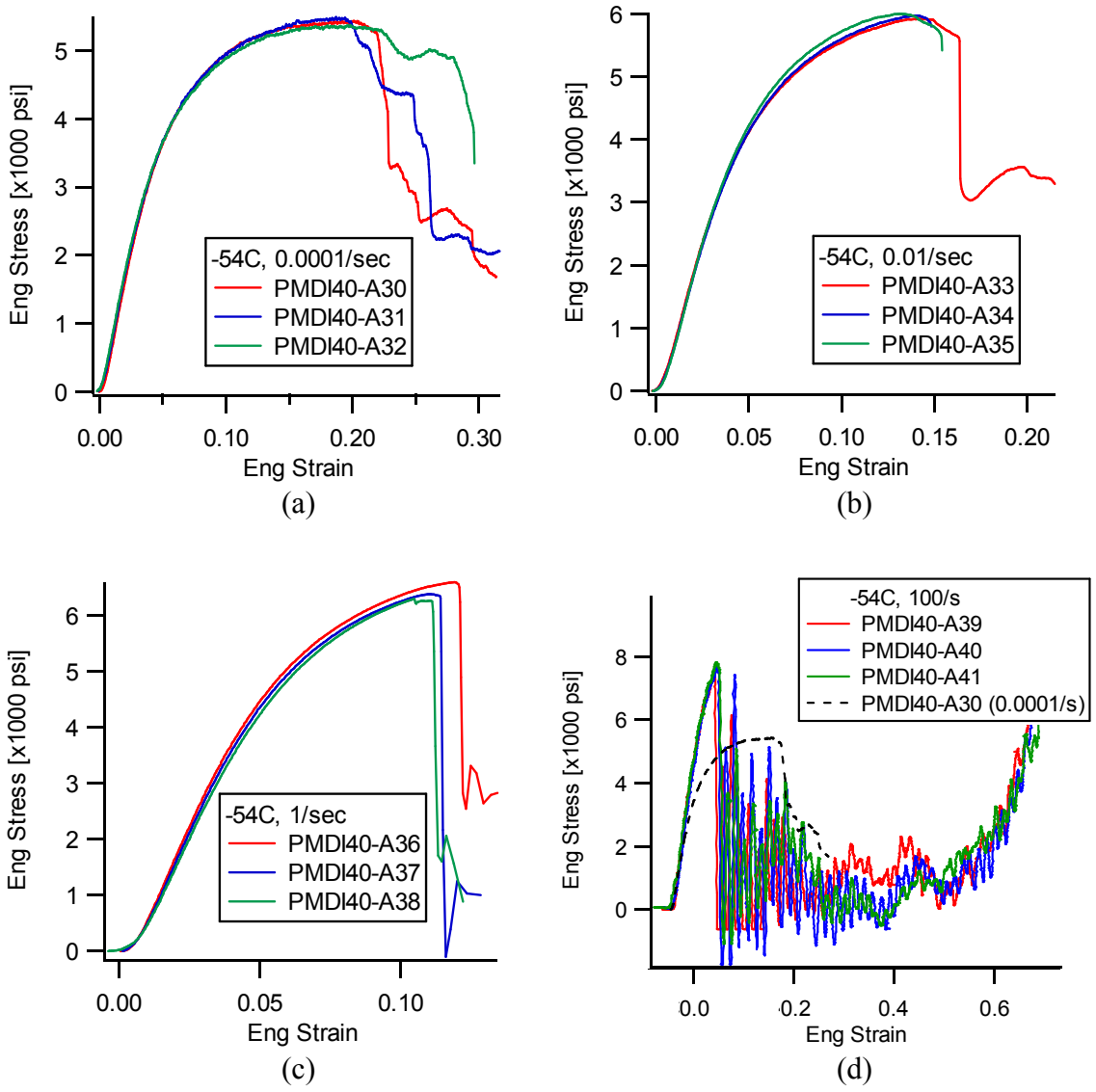

Figure 13 Engineering stress-stress relations of PMDI40 at -65°F for various strain rates (a) 0.0001/s, (b) 0.01/s, (c) 1.0/s, and (d) 100/s.

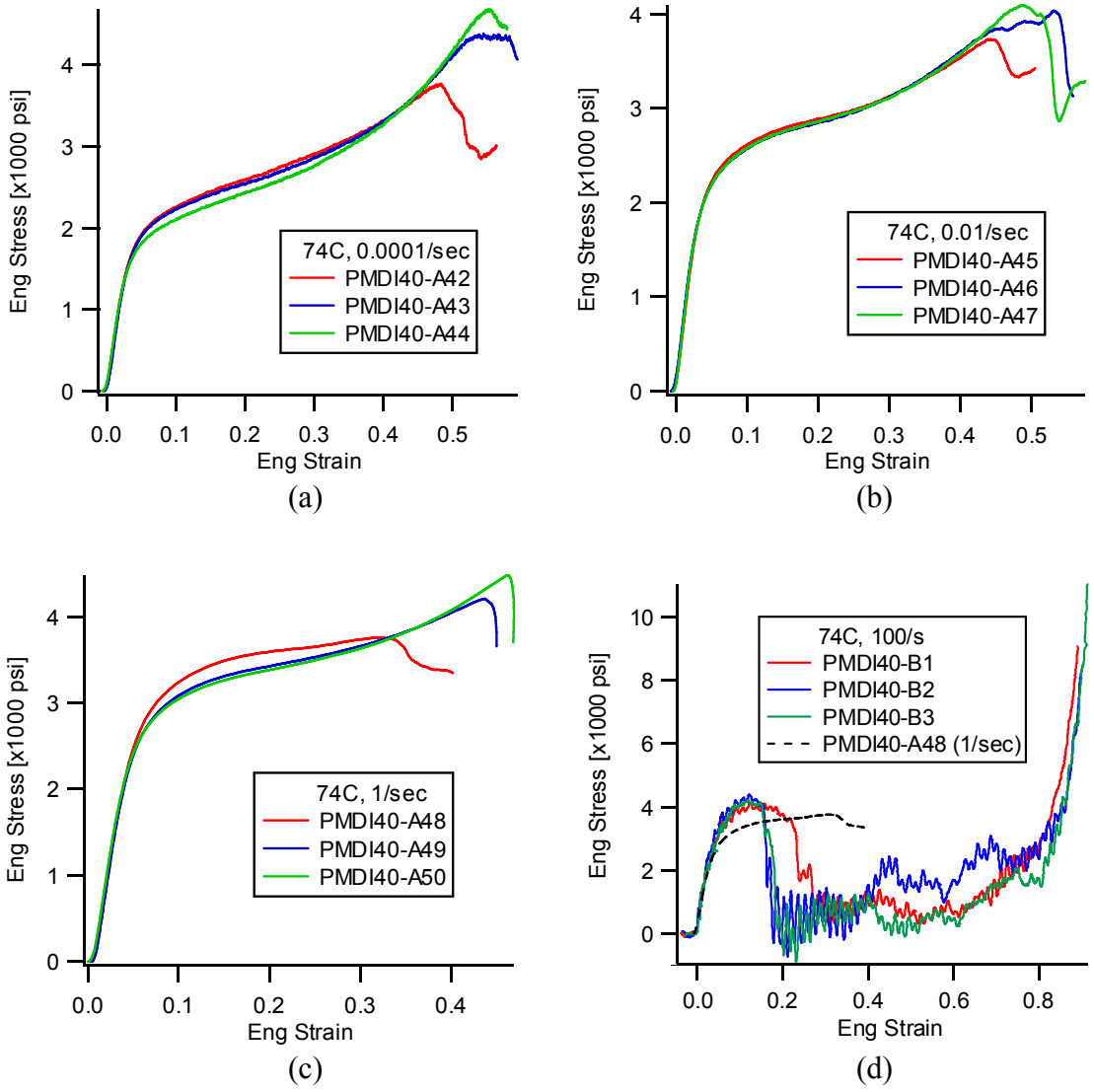

Figure 14 Engineering stress-stress relations of PMDI40 at 165°F for various strain rates (a) 0.0001/s, (b) 0.01/s, (c) 1.0/s, and (d) 100/s.

2.2.4.1. Effects of Lubricant and Specimen Aspect Ratio

The lubricant and aspect ratio issues have been studied in section 2.2.2.1. The study here repeats similar experiments for PMDI40. Additional specimens were made, which had a constant height of 0.5 inch but diameter changed from 0.405 to 0.756 inch, Table 6.

Results are shown in Fig. 15. Again, the specimen aspect ratio and lubrication have little effect on the stress-strain behavior. It is consistent with the previous observation.

Table 6 Additional 40 pcf PMDI foam specimens

Specimen	Diameter (in.)	Height (in.)	Density (pcf)	Temperature (degree F)	Rate (s^{-1})	Lubricant	Aspect Ratio
A4	0.756	0.497	33.69	70	0.01	No	0.7
A5	0.755	0.497	33.79	70	0.01	No	0.7
A6	0.756	0.500	34.44	70	0.01	Yes	0.7
A7	0.757	0.500	33.90	70	0.01	Yes	0.7
A10	0.519	0.500	33.91	70	0.01	No	1.0
A11	0.517	0.500	34.25	70	0.01	No	1.0
A12	0.519	0.498	33.95	70	0.01	Yes	1.0
A13	0.520	0.503	33.75	70	0.01	Yes	1.0
A15	0.402	0.500	33.71	70	0.01	No	1.2
A16	0.405	0.495	34.67	70	0.01	No	1.2
A17	0.405	0.501	34.44	70	0.01	Yes	1.2
A18	0.405	0.505	34.12	70	0.01	Yes	1.2

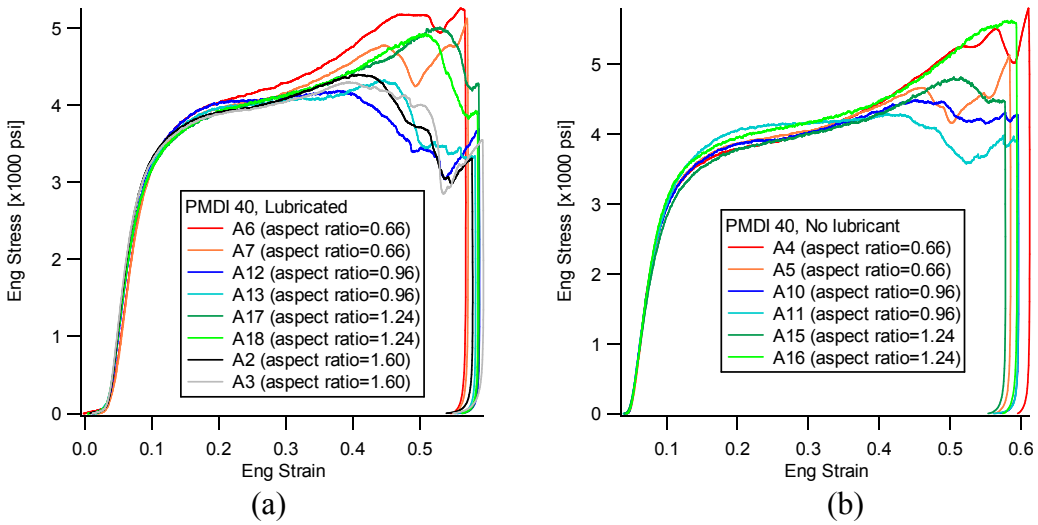

Figure 15 Effects of lubricant and specimen aspect ratio.

2.2.5. PMDI50

A limited set of experiment was conducted for PMDI50, only one strain rate 0.01/s was considered. Table 7 lists the test matrix and Fig. 16 shows engineering stress-strain results.

2.2.6. TufFoam35

TufFoam35 had a similar set of tests as PMDI50. Test matrix and results are shown in Table 8 and Fig. 17. The TufFoam35 and PMDI40 specimens turned out to have the same measured density. Considering the same testing condition at 70^{o}F and 0.01/s, Figs. 12(b) and 17, the crush stresses were about 3.8 and 3.4 ksi, and fail strains were about 40% and 65% for PMDI40 and TufFoam35, respectively. TufFoam35 appears to be more ductile but crushes at a lower stress.

2.2.6.1. Loading-unloading-reloading

Specimen U07 had a different loading profile. Instead of compressing monotonically, it had several cycles of unloading and reloading. The result is plotted along with the monotonically loaded specimens in Fig. 17(d). The unloading-reloading curve shows several interesting features. It is bounded by the monotonic compression curve as the yield stress. When reloading beyond reaching the yield stress, the stress-strain curve follows the monotonic compression curve just like a typical plasticity material. The unloading-reloading curve within the yield surface forms a loop; it behaves like a viscoelastic material. As the crush strain increases, the loop gets more tilted and bigger, which indicates the storage modulus becomes smaller but the loss modulus turns out to be larger.

2.2.6.2. TufFoam35 Batch 2

For the second batch, each specimen was molded individually. The size was much larger and the aspect ratio was smaller. Table 9 lists the test matrix and specimens. To handle these large specimens a different setup, different from the one described in Fig. 1, was necessary. A MTS 220 kips system was used for this set of experiment. Figure 18(a) shows the setup without an environmental chamber so the loading train can be seen easily. The environmental chamber was modified to have a transparent door to allow optical strain measurement at different temperatures, Fig. 18(b).

Figure 19 shows engineering stress-strain results. Notice that the strain rates for Batch 1 and 2 specimens were not the same, Batch 2 specimens were loaded with a strain rate that was an order of magnitude slower. Only two temperature conditions, room temperature and high temperature, were included. In the figure, TufFoam35 Batch 1 results are also plotted for comparison. The density of Batch 2 specimens was slightly higher, but the crush stress was lower. Factoring in the strain rate effect, the properties of these two batches are reasonably consistent. This can be estimated from the strain rate effects of PMDI40 specimens plotted in Fig. 20 since both TufFoam35 and PMDI40 specimens had the same density.

Table 7 Test matrix of uniaxial compression of 50 pcf PMDI foam

Specimen	Diameter (in.)	Height (in.)	Density (pcf)	Temperature (degree F)	Rate (s^{-1})
A1	0.606	1.192	50.99	70	0.01
A2	0.598	1.208	50.66	70	0.01
A3	0.600	1.196	50.98	70	0.01
B2	0.500	1.000	48.87	-65	0.01
B3	0.504	0.930	47.77	-65	0.01
B5	0.503	0.510	47.93	165	0.01
B6	0.502	0.505	47.79	165	0.01
B7	0.502	0.504	47.72	165	0.01

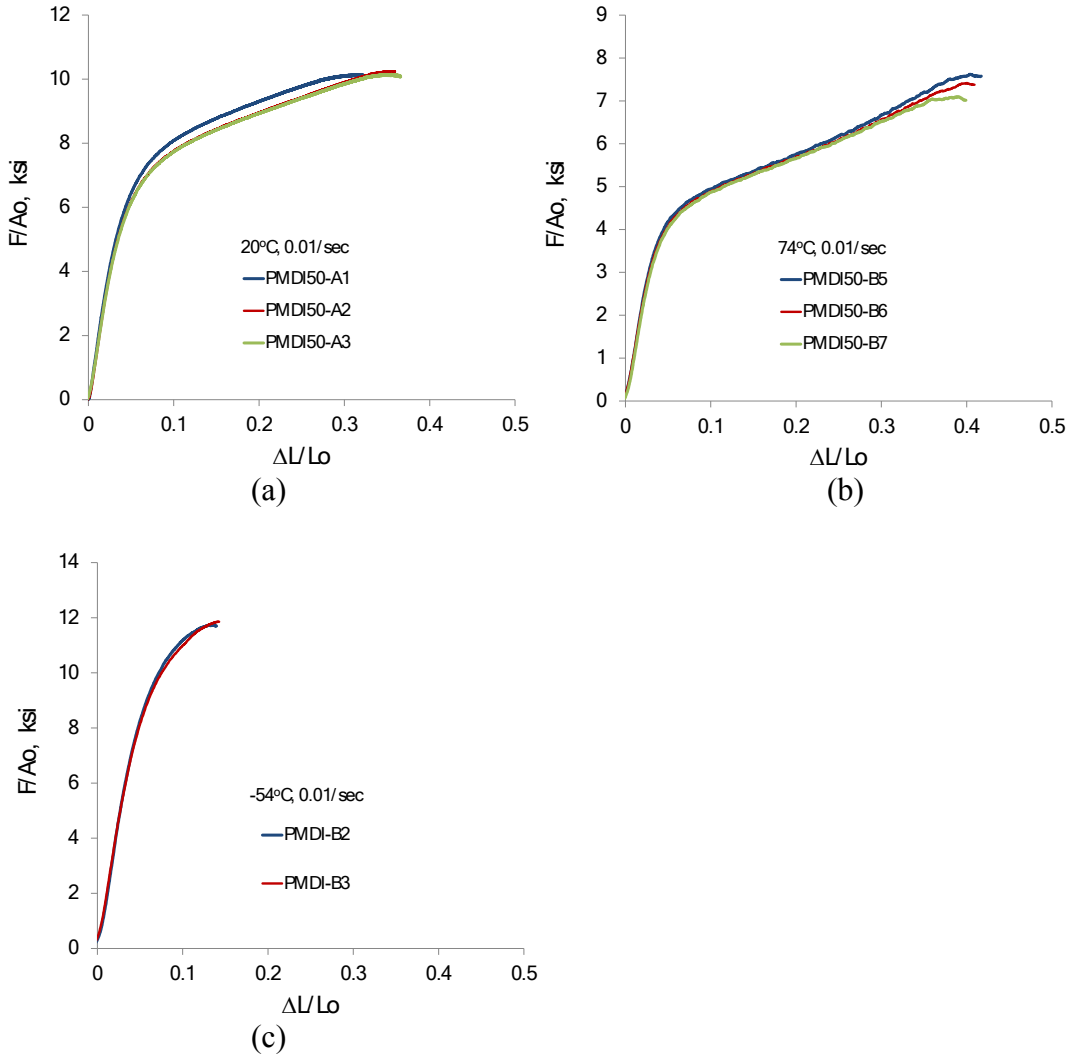

Figure 16 Stress-stress relations of PMDI50 at (a) 70°F, (b) 165°F, and (c) -65°F.

Table 8 Test matrix of uniaxial compression of 35 pcf TufFoam

Specimen	Diameter (in)	Hight (in)	Density (pcf)	Temperature (degree F)	Rate (s^{-1})
U01	1.050	1.014	34.10	70	0.01
U02	1.048	1.012	34.65	70	0.01
U03	1.049	1.015	34.31	70	0.01
U04	1.051	1.013	34.46	165	0.01
U05	1.048	1.012	34.39	165	0.01
U06	1.050	1.014	34.36	165	0.01
U07	1.049	1.014	34.47	165	0.01
U08	1.048	1.013	34.53	-65	0.01
U09	1.052	1.012	34.08	-65	0.01
U10	1.050	1.015	34.07	-65	0.01

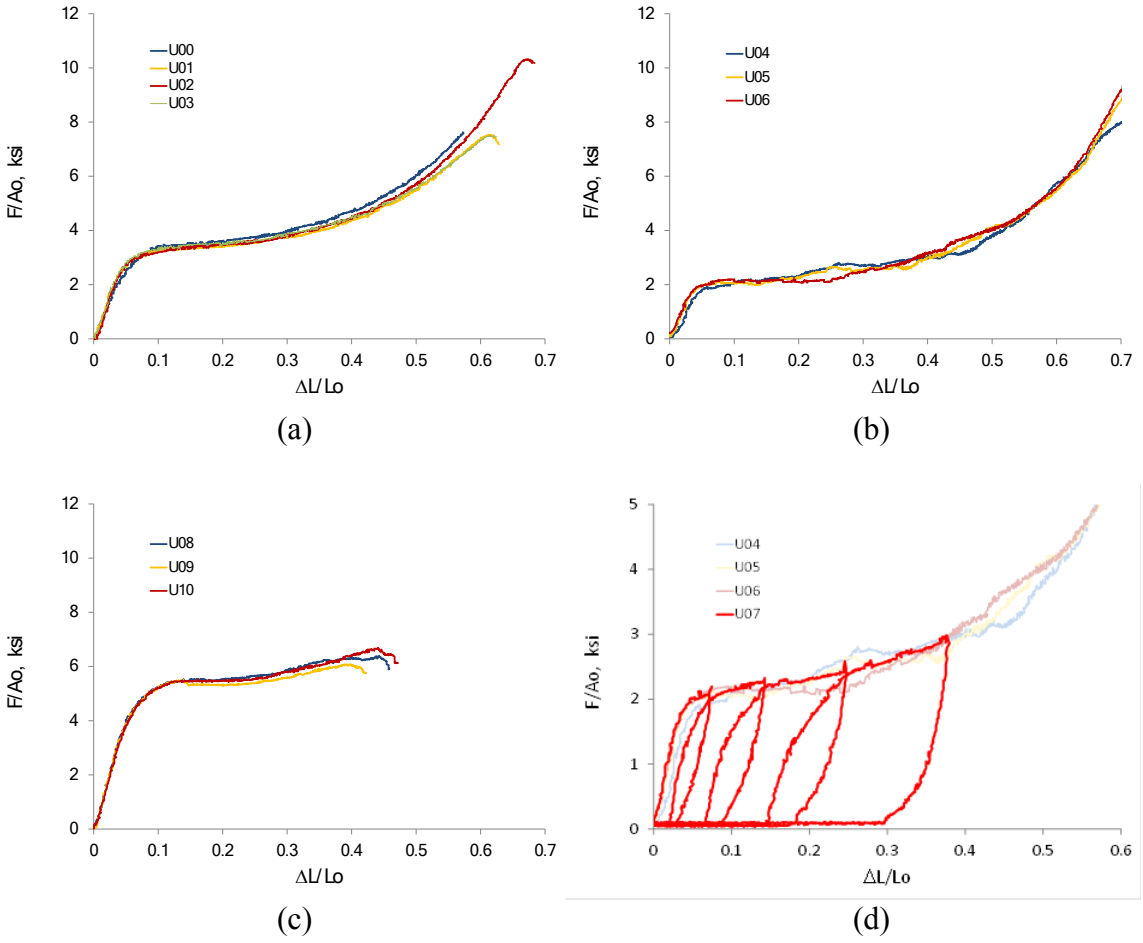

Figure 17 Stress-stress relations of TufFoam35 at (a) 70°F, (b) 165°F, and (c) -65°F.

Table 9 Compression of second batch TufFoam35

Specimen	Diameter (in)	Hight (in)	Density (pcf)	Temperature (degree F)	Rate (s^{-1})
35-S-RT-1	4.855	2.5	35.10	68	0.001
35-S-RT-2	4.855	2.5	35.10	68	0.001
35-S-RT-3	4.855	2.5	35.10	68	0.001
35-S-HT-1	5.000	2.5	35.91	175	0.001
35-S-HT-2	5.000	2.5	35.20	175	0.001
35-S-HT-3	5.000	2.5	36.61	175	0.001

(a) (b)

Figure 18 Compression setup on MTS 220 kips system.

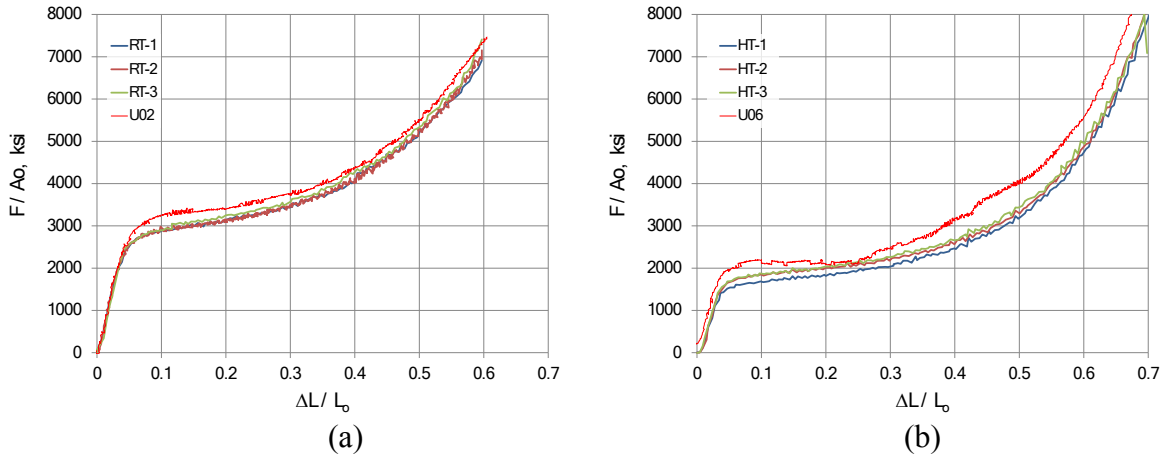

Figure 19 Stress-stress relations of 2nd batch TufFoam35 at (a) 70°F, and (b) 165°F.

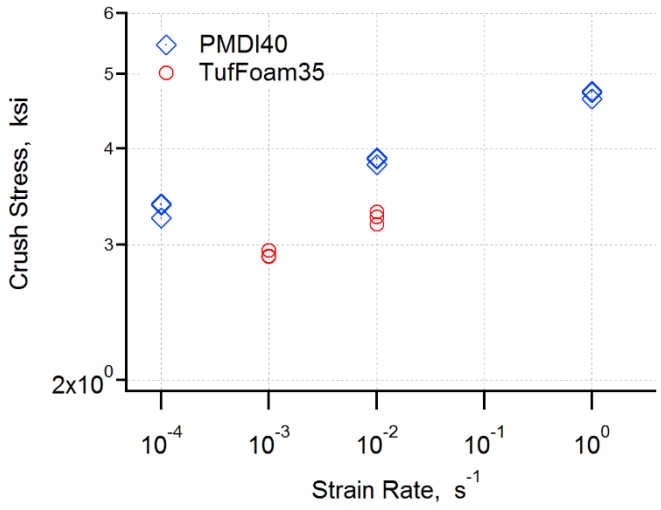

Figure 20 The strain rate effect of PMDI40 specimens.

2.2.7. TufFoam65

TufFoam65 specimens were also molded individually. The tests were performed on the 220 kips system. The test matrix of TufFoam65 was listed in Table 10. Initially, the diameter of the specimen was 5 inch. The required load to crush the specimen, however, was higher than the capacity of the system, so the diameter of all specimens was modified to 4 inch.

Experimental results are shown in Fig. 21. Specimen 65-S-RT-3 experienced some unloading-reloading cycles. Similar to TufFoam35 Batch 1 specimen U07, it exhibits yield stress and plasticity behavior during loading and is viscoelastic when unloading and reloading before yield.

Table 10 Compression of TufFoam65

Specimen	Diameter (in)	Height (in)	Density (pcf)	Temperature (degree F)	Rate (s^{-1})
65-S-RT-1a	5.0	1.5	64.00	70	0.001
65-S-RT-1b	4.0	1.5	63.10	70	0.001
65-S-RT-2	4.0	1.5	65.10	70	0.001
65-S-RT-3	4.0	1.5	61.40	70	0.001
65-S-HT-1	4.0	1.5	64.17	175	0.001
65-S-HT-2	4.0	1.5	64.17	175	0.001
65-S-HT-3	4.0	1.5	62.34	175	0.001

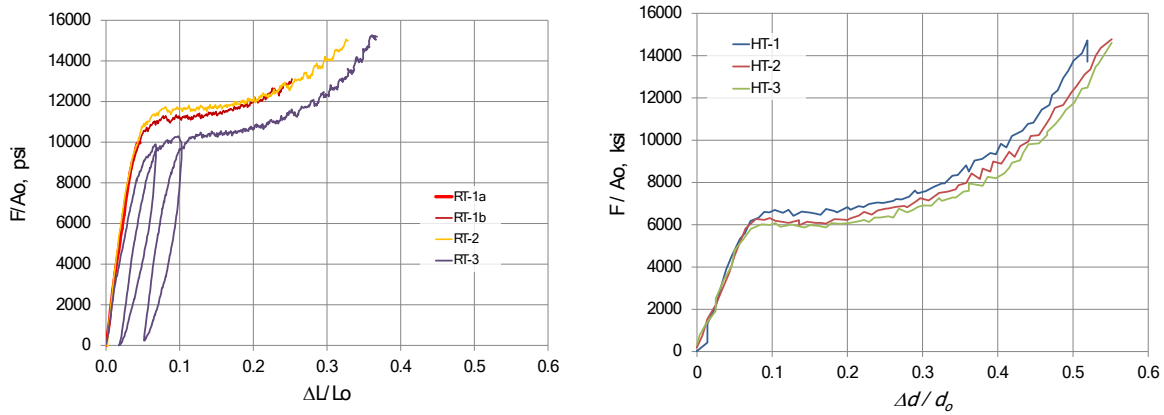

Figure 21 Stress-stress relations of TufFoam65 at (a) 70°F, and (b) 165°F.

2.3. Effects of Density

The compressive stress-strain behaviors of foams of various densities were presented. Their crush stress and initial elastic modulus are quantitatively summarized with respect to the density in Figs. 22 and 23, respectively. The crush stress is the stress value at the beginning of the plateau region, about at 0.1 – 0.15 of strain.

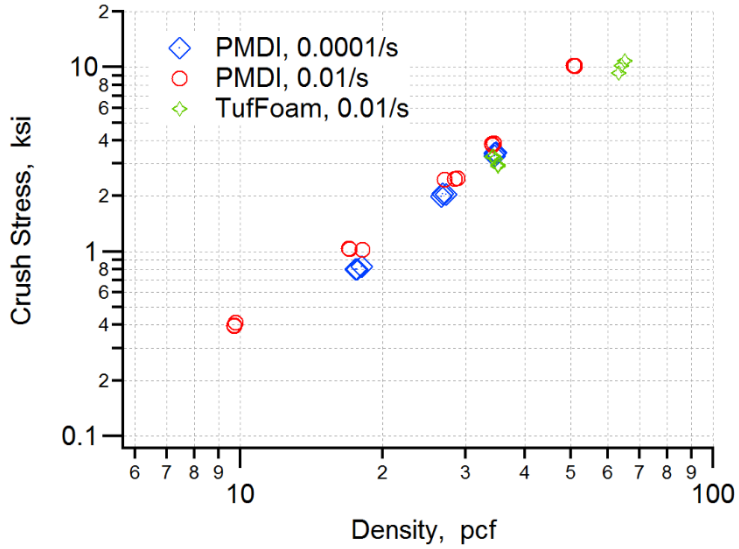

Figure 22 The density effect on crush stress.

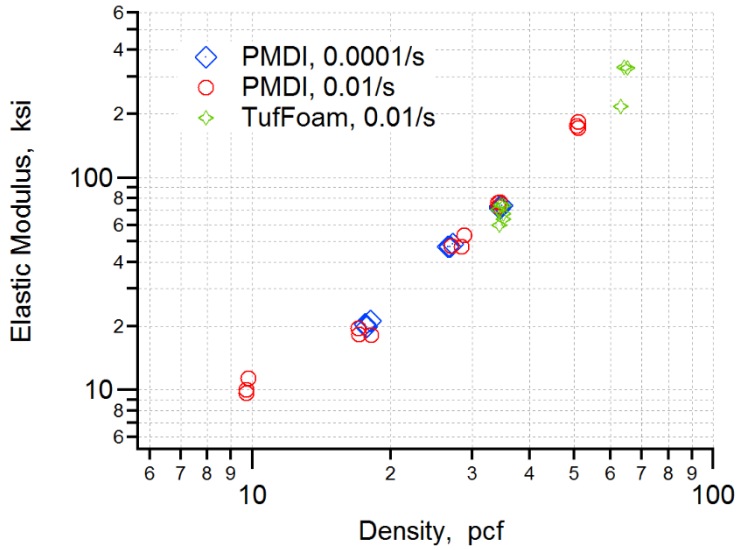

Figure 23 The density effect on initial elastic modulus.

3. CONFINED COMPRESSION

3.1. Rigid Confinement

Thick-wall chamber was used to prohibit displacements in the transverse directions. Since high rate strain loading, on the order of 10^2/s, was considered, attaching the chamber and load washers on the crosshead, which was stationary, was necessary. Frictions on the chamber wall needed to be subtracted.

3.1.1. Experimental Methods

The schematic of the experimental setup is shown in Fig. 24(a). The axial compressive force F_{com} of the foam is transmitted through the platen to the adaptor, while the friction force F_f is transmitted through the confined chamber and load washer #2 to the adaptor. Load washer #1 measures the total force F_{total} (= F_1) that is the sum of the axial compressive force and the friction force, that is

$$F_{total} = F_{com} + F_f \text{ (or } F_{com} = F_1 - F_f) \tag{1}$$

Notice load paths of F_{com} and F_f are independent. The platen is connected to the adaptor directly and does not touch the confined chamber or load washer #2. Ideally, load washer #2 directly gauges F_f if the adaptor is rigid. The deformation of the adaptor, however, affects the measurement of load washer #2, i.e. F_2. This cross talk from F_{com} needs to be calibrated.

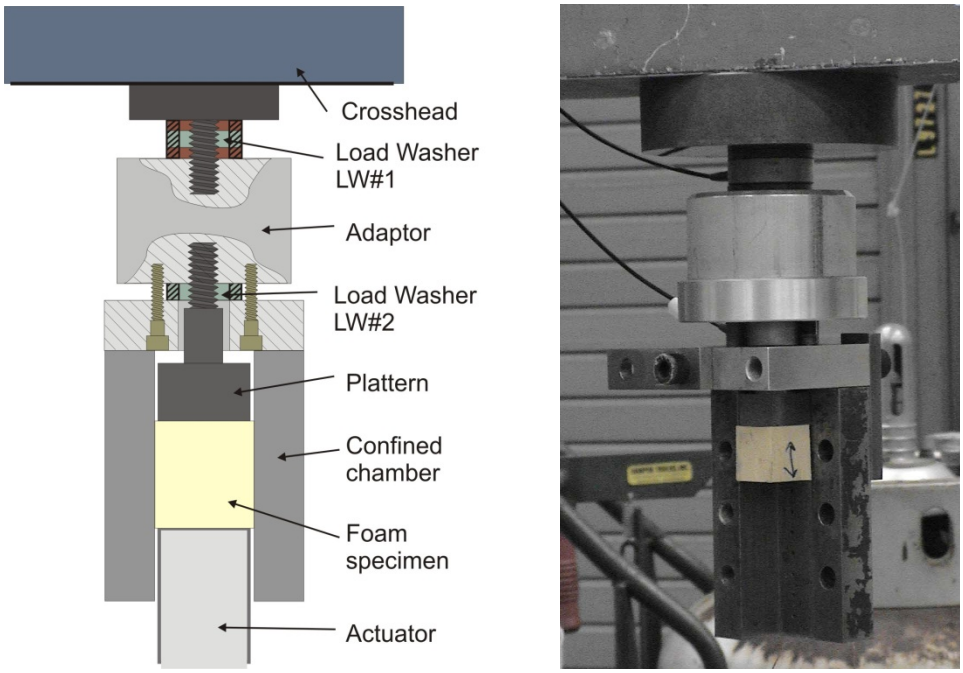

Figure 24 Experimental Setup for foam rigid confined compression.

The calibration was done by applying the force at the chamber only and at the platen only. The following relation was obtained to calculate the friction force:

$$F_f = 0.0069\, F_1^2 - 0.1298\, F_1 - F_2 \qquad (2)$$

The foam compression force F_{com} was calculated from (1).

3.1.2. Experiment and Results

Two foams were tested under the rigid confinement: PMDI20 and TufFoam35.

3.1.2.1. PMDI20

The test set is listed in Table 11. Using Specimen 2 as an example, the measured and calculated quantities are plotted in Fig. 25. The left and right axes are stroke and force, respectively. The averaged axial stress-strain curves are shown in Fig. 26 and 27 for room temperature and low temperature tests. Under the rigid confinement, failure will not happen; also, the crush stress is much higher than the uniaxial compression, Figs. 3 an 4. Notice that there is a 10% difference in density among specimens of -65^{o}F and 125/s test; the stress-strain curves appear in two separated groups according to the density, Fig. 27(b).

Table 11 Test matrix of rigid confined compression of PMDI20 foam

Specimen	Width (in)	Thickness (in)	Length (in)	Density (pcf)	Temperature (degree F)	Strain Rate (s^{-1})
1	1.246	1.242	1.508	22.8	70	0.06
2	1.254	1.253	1.501	23.1	70	0.01
3	1.249	1.246	1.498	23.7	70	0.01
4	1.244	1.243	1.500	22.7	70	0.01
5	1.243	1.245	1.502	22.7	70	125.00
6	1.239	1.246	1.502	22.6	70	123.00
7	1.247	1.249	1.501	22.6	70	124.00
8a	1.224	1.224	1.497	23.4	-65	125.00
8	1.223	1.222	1.495	23.9	-65	125.70
9	1.224	1.222	1.489	20.9	-65	129.67
10	1.221	1.223	1.485	21.5	-65	132.78
12	1.223	1.223	1.490	20.7	-65	0.01
13	1.216	1.221	1.490	20.6	-65	0.01
14	1.220	1.222	1.490	20.7	-65	0.01
15	1.222	1.220	1.489	20.9	-65	0.01

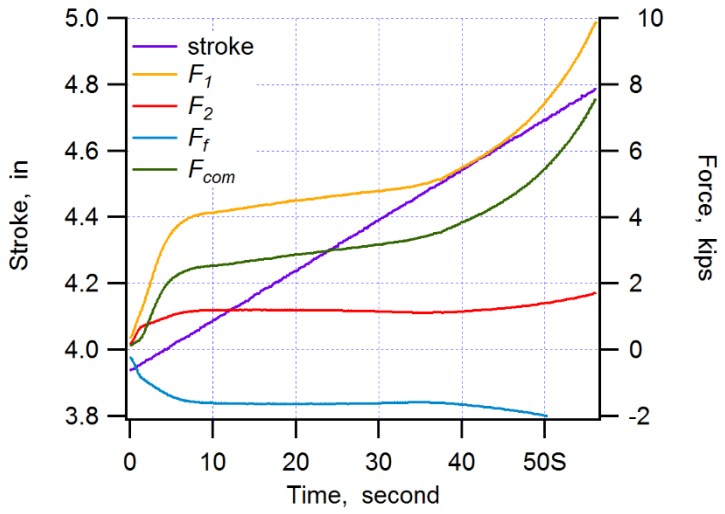

Figure 25 Histories of forces and displacement of rigid confined Specimen 2.

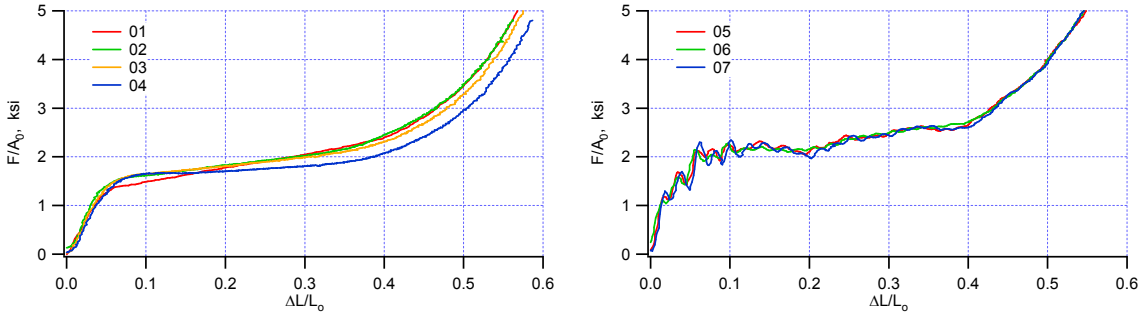

Figure 26 PMDI20 rigid confined compression at 70°F, (a) Strain rate 0.01/s and (b) Strain rate 125/s.

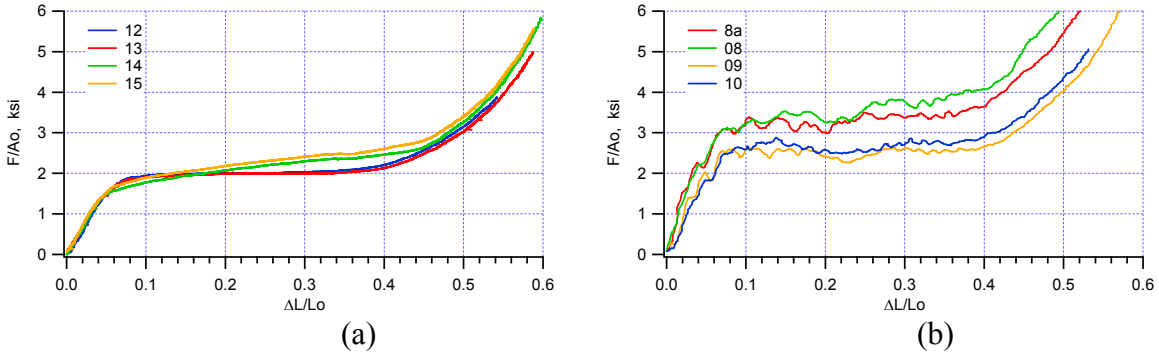

Figure 27 PMDI20 rigid confined compression at -65°F, (a) Strain rate 0.01/s and (b) Strain rate 125/s.

3.1.2.1. TufFoam35

Table 12 lists the test condition and specimens. The results are in Fig. 28.

Table 12 Test matrix of rigid confined compression of TufFoam35

Specimen	Width (in)	Thickness (in)	Height (in)	Density (pcf)	Temperature (degree F)	Rate (s^{-1})
C01	1.200	1.200	1.506	33.99	70	0.01
C02	1.198	1.207	1.482	34.45	70	0.01
C03	1.205	1.202	1.510	34.05	70	0.01

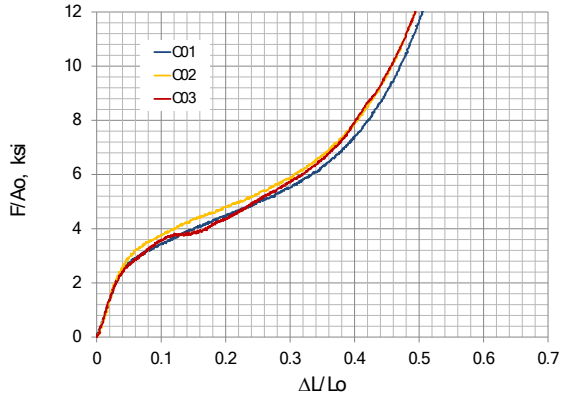

Figure 28 TufFoam35 rigid confined compression at 70°F.

3.2. Elastically Confined Compression

3.2.1. Experimental Method

The schematic of the experimental setup is shown in Fig. 1. A load washer is mounted between the crosshead and the top push rod and, similarly, a load cell is set in between the actuator and the lower push rod to measure the respective forces F_w and F_c applied to the foam sample. A thin wall tube, 0.10 inch thick, made of Al7075-T7351 is supported by a structure fixed on the crosshead. The clearance between the tube and push rod is about 0.005 inch. The foam specimen is snug inside the tube. Strain gages are mounted on the tube to measure the hoop strain history. It is 1/8" from the location where the top of the foam is placed. Diametric extensometer has also been used to measure the stain. The whole assembly is enclosed by an environmental chamber on a MTS testing frame.

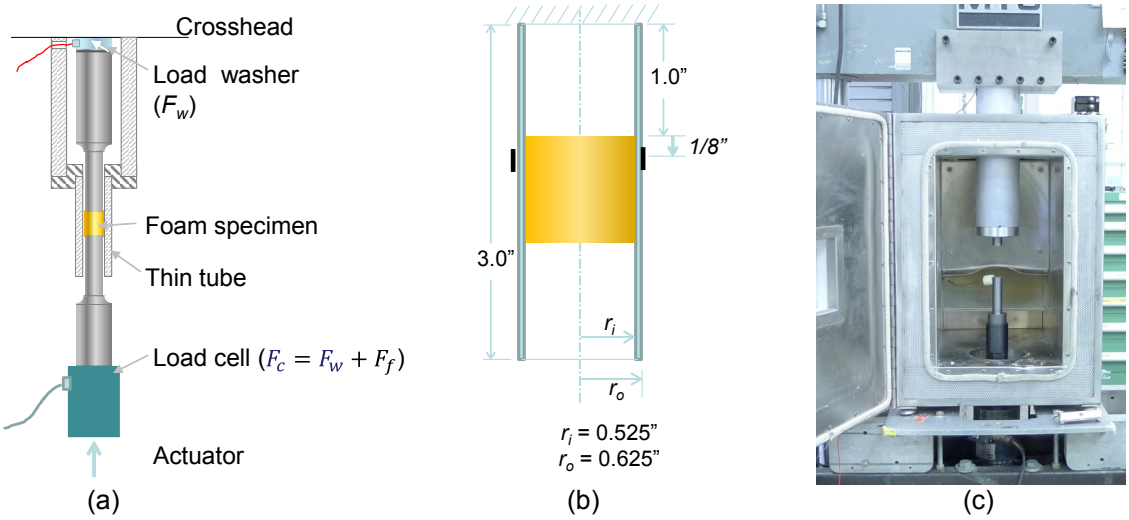

Figure 29 Foam elastically confined compression: (a) schematic, (b) thin-wall tube design, and (c) system setup.

3.2.2. Room Temperature Results

3.2.2.1. TufFoam35

The first foam material of interest is TufFoam35. The histories of measured displacement, force and hoop strain of a typical test, Specimen 18, are plotted in Fig. 30. Specimens were compressed under a constant speed of 0.002 in/s, Fig. 30(a). The compressive force measured from the actuator side F_c is generally greater than the force measured by the load washer F_w at the crosshead, Fig. 30(b). The difference is the friction force at the tube wall, that is

$$F_c = F_w + F_f \tag{3}$$

In this test, the hoop strain was measured by two strain gages and a diametric extensometer. All three values were consistent, Fig. 30(c), and an average of three curves is also plotted.

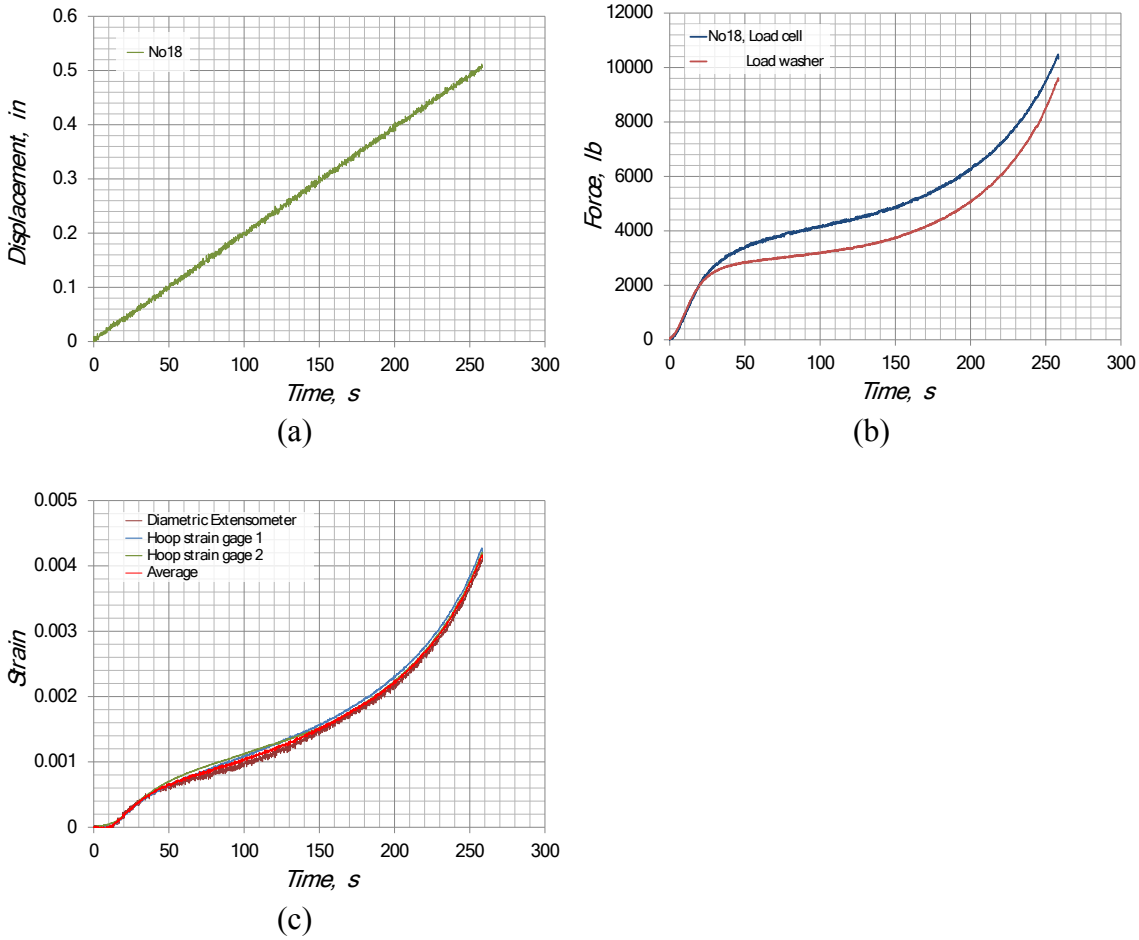

Figure 30 Histories of a typical elastically confined compression of TufFoam35, specimen 18: (a) displacement, (b) axial force, and (c) hoop strain.

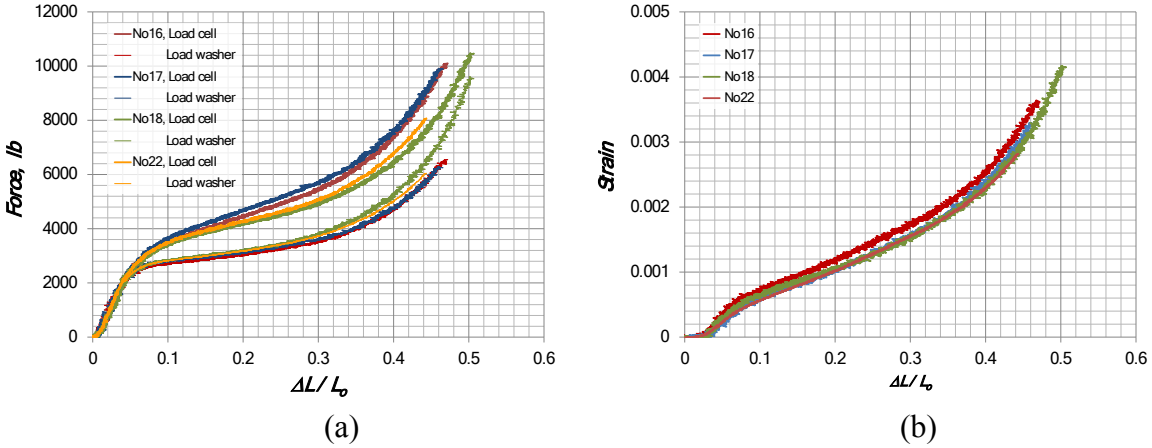

Figure 31 Elastically confined compression of TufFoam35, (a) force, and (b) hoop strain.

Four repeats were conducted for TufFoam35. Forces and strains versus the averaged axial strain are summarized in Fig. 31. In the first two tests, Specimens 16 and 17, the foam-tube interface was not lubricated; the other two tests, Specimens 18 and 22, the interface was lubricated with a thin layer of Corning vacuum grease. It is clear in Fig. 31(a) that with lubrication the gap between F_c and F_w becomes narrower; it makes F_c smaller and F_w larger. It also lowers the hoop strain at the measuring location, Fig. 31(b).

3.2.2.2. PMDI50

Forces and strains versus axial strain are plotted in Fig. 32(a) and (b), respectively. To keep the deformation of the aluminum tube within the elastic limit, the averaged axial strain was small, less than 15%.

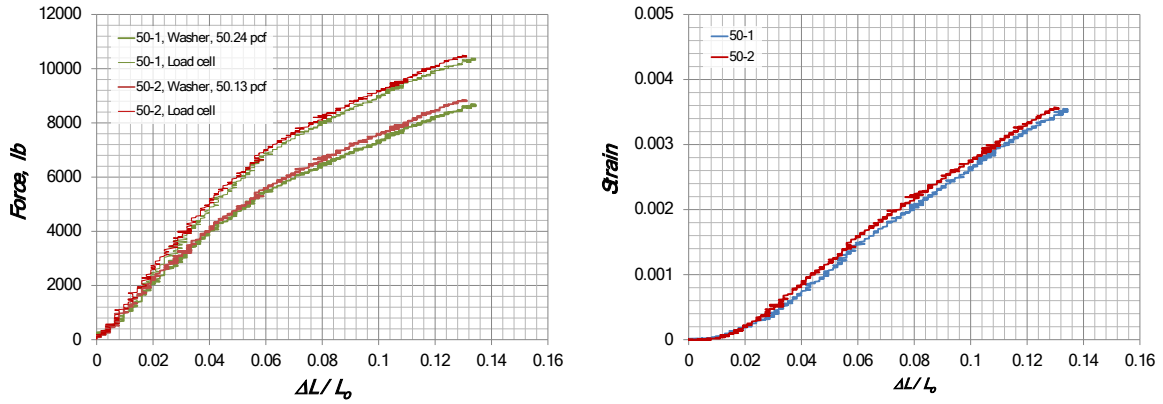

(a) (b)

Figure 32 Elastically confined compression of PMDI50, (a) force, and (b) hoop strain.

3.2.2.3. PMDI40

Experimental results are plotted in Fig. 33.

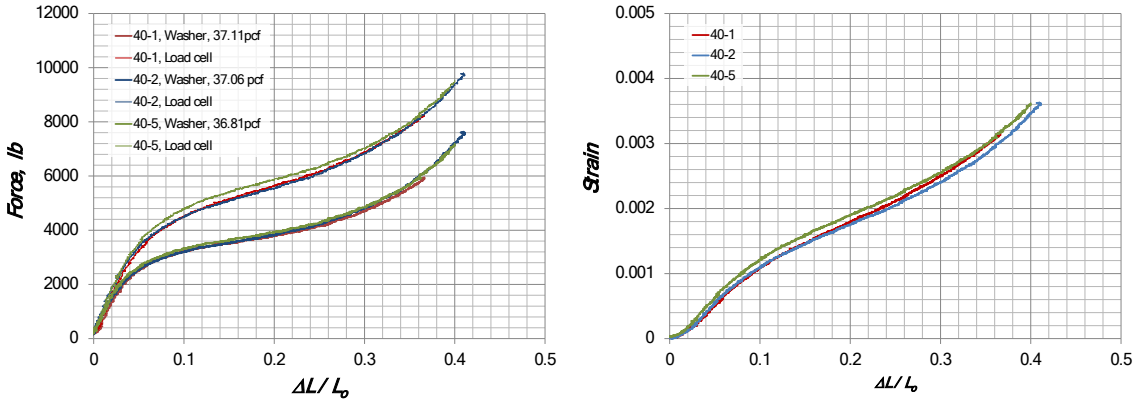

(a) (b)

Figure 33 Elastically confined compression of PMDI40, (a) force, and (b) hoop strain.

3.2.2.4. PMDI30

Only one test was conducted, Fig. 34. The hoop strain did not increase until about 2% of axial strain, Fig. 34(b). It indicates that the specimen fit loosely inside the tube. The initial volume gap between the specimen and the chamber in a confined compression is a parameter that is difficult to quantify experimentally. It can be estimated by numerical simulation.

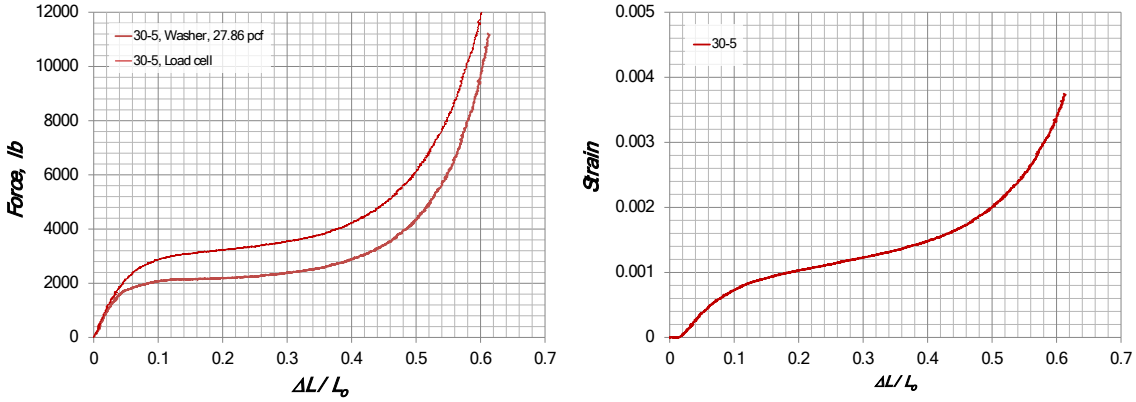

(a) (b)

Figure 34 Elastically confined compression of PMDI30, (a) force, and (b) hoop strain.

3.2.2.5. PMDI20

Results are shown in Fig. 35. As the foam density is lower, the difference between F_c and F_w is less, Fig. 35(a). The hoop strain is smaller. With the same resolution and the relative error becomes significant, Fig. 36.

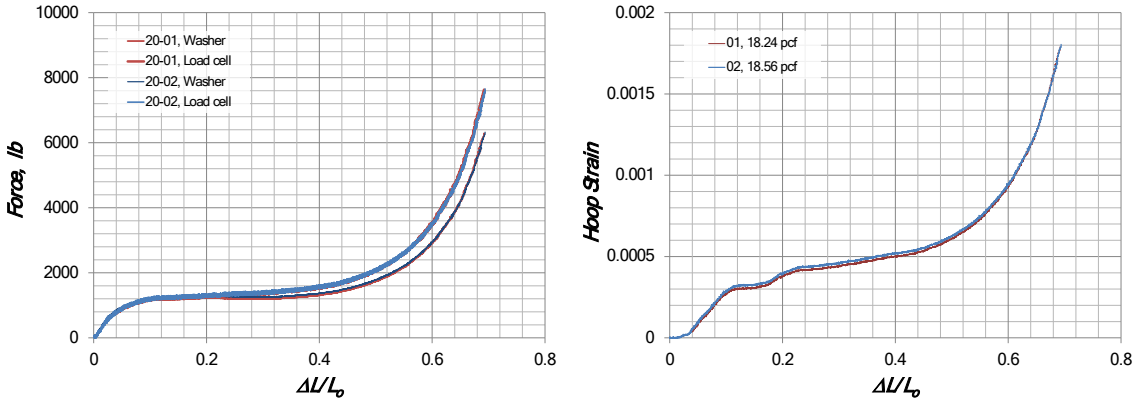

(a) (b)

Figure 35 Elastically confined compression of PMDI20, (a) force, and (b) hoop strain.

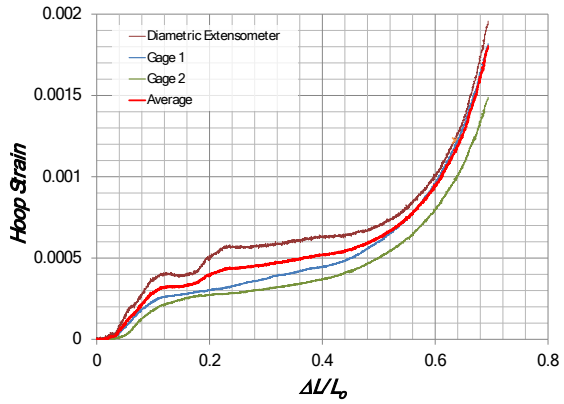

Figure 36 Hoop strain histories of PMDI20-01.

3.2.2.6. PMDI10

For PMDI10, the measured forces were the same, Fig. 37(a); but the hoop strain was too small to measure for the tube, Fig. 37(b). A more sensitive tube is needed for lower density foams.

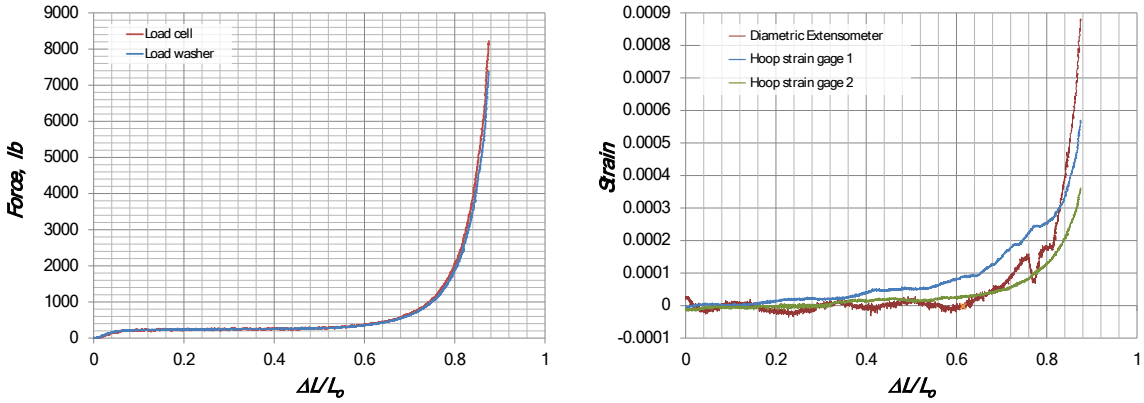

Figure 37 Elastically confined compression of PMDI10, (a) force, and (b) hoop strain.

3.2.3. Thin Tube

A thin tube is designed to have a high sensitivity for measuring low internal pressure cases, Fig. 38(a). It basically has the same dimensions as the first tube, Fig. 29, so it is compatible with the setup, Fig. 38(c). The only modification is that at the mid testing section, the outer diameter reduces to 1.091 inch. Four strain gages are mounted and separated evenly along the hoop direction, Fig. 38(b). Diametric extensometer is not used in this design.

Figures 39 and 40 present the experimental results of PMDI20 and PMDI10, respectively, utilizing the thin tube. Data are still scattered, but with a better resolution.

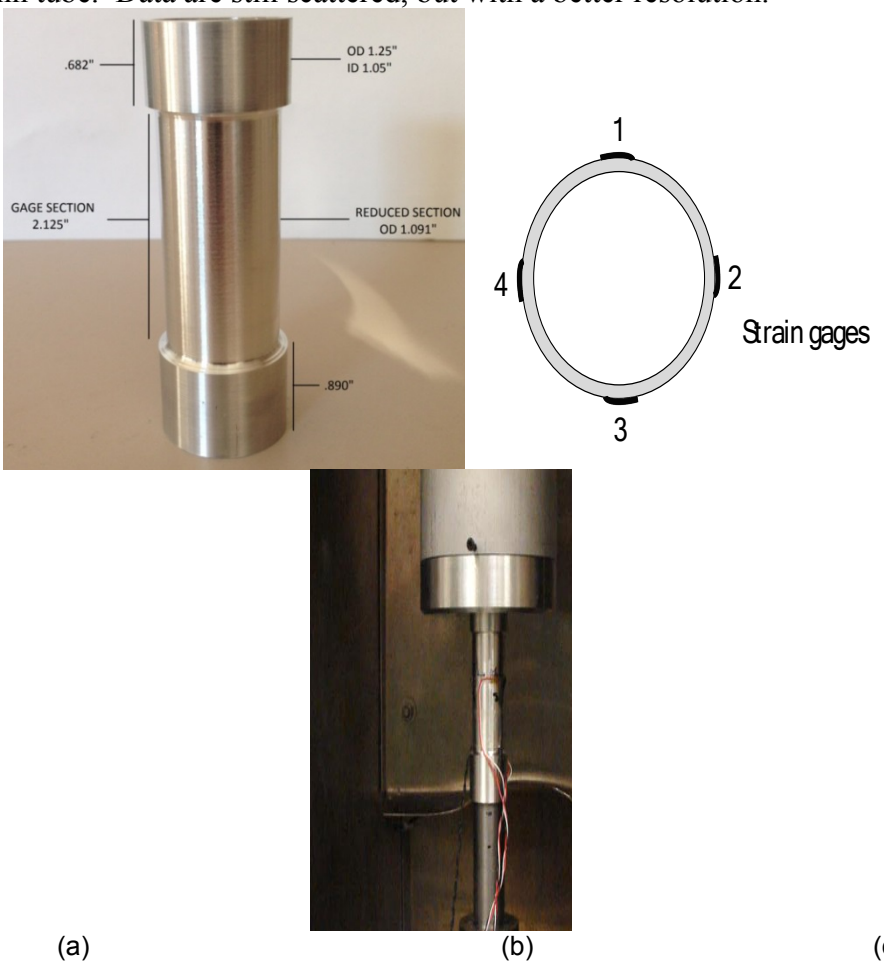

Figure 38 Thin tube for elastically confined experiment of low density foams: (a) tube design, (b) location of strain gages, and (c) testing setup.

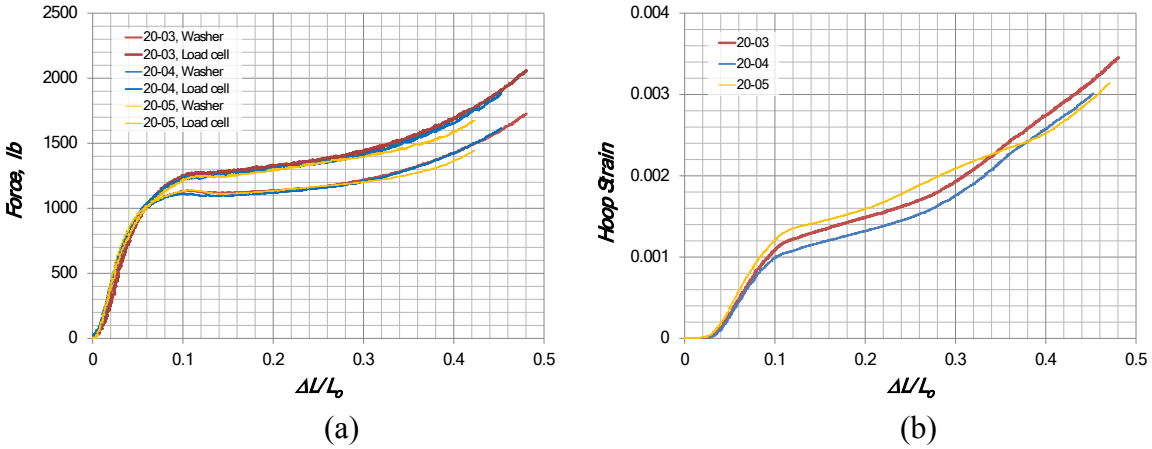

Figure 39 Thin-tube confined compression of PMDI20, (a) force, and (b) hoop strain.

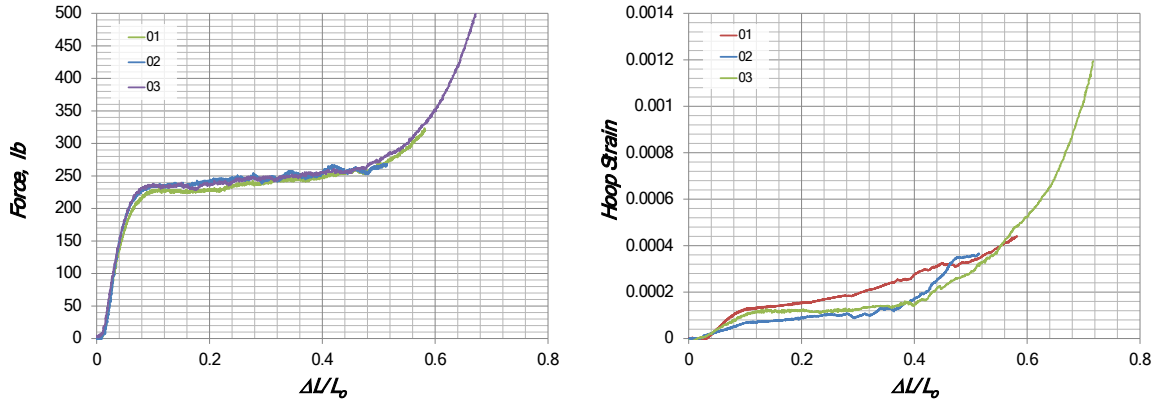

Figure 40 Thin-tube confined compression of PMDI10, (a) force, and (b) hoop strain.

3.2.4. High Temperature Experiment of TufFoam35

The newly developed elastically confined compression was also applied to TufFoam35 at elevated temperature 170°F. Results are displayed in Fig. 41.

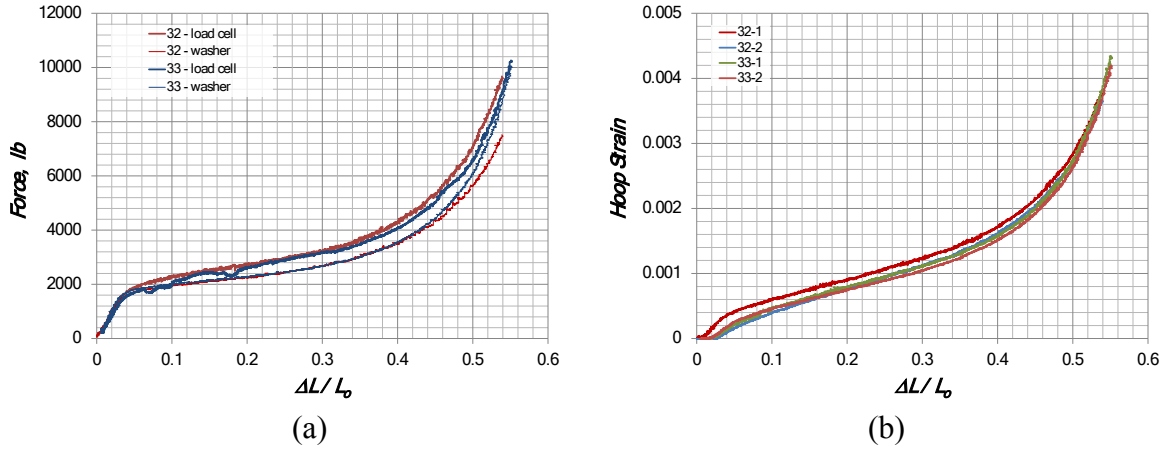

Figure 41 Confined compression of TufFoam35 at 170°F, (a) force, and (b) hoop strain.

3.2.4. Discussion

These new experimental data were applied to calibrate a model parameter, beta, which defines the inelastic flow direction as some combination of radial and associated flow [1]. When beta is equal to 1.0, purely radial flow (flow direction given by normalized stress tensor) is used; when beta is equal to 0.0, purely associated flow is used; and for beta, β, values between 0 and 1, a normalized linear combination of associated and radial flow is used. Previous studies by Zhang et al. [4], suggested that the inelastic flow direction would be almost purely radial. These experiments, however, reveal that for high density foams the inelastic flow direction is associated, and that only for low density foams at small strains is the flow direction closer to radial. For example, using β=0.9 will severely under predict the hoop strain of TufFoam35 under confined compression. Only by adjusting the β value to zero, the model simulation

matches the experimental data over the crush region, approximately between t = 30 to 200 s, as shown in Fig. 42(a). The difference between the experiment and simulation during the first 30 seconds is possibly due to the loose fit between the sample and the tube.

It is also necessary to adjust the model parameters of PMDI20 to match its experimental response, Fig. 42(b). A function $\beta(\square)$ is obtained for the material, shown in Fig. 43. It suggests that the flow direction is dependent on the volume fraction of solid material, $\square$.

3.2.5. Conclusion

Confined compression provides critical data for calibrating foam model parameters. The data show the flow direction depends on the foam density: associate flow for high density foams (35 pcf); for lower density foams PMDI20 pcf, it starts with non-associate flow and changes to associate flow as the foam crushed and became denser. There may be a universal curve for flow direction as a function of phi that applies to all rigid polyurethane foams, which needs further investigation.

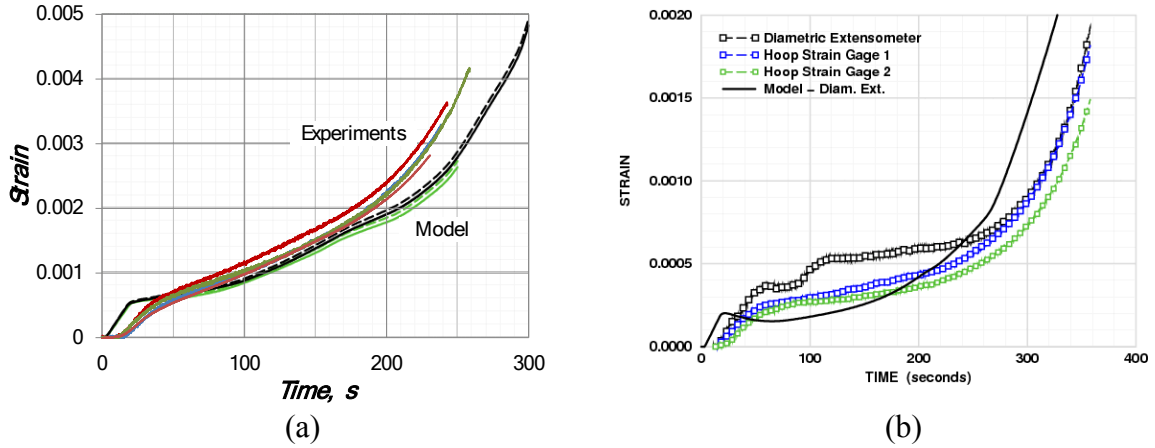

Figure 42 Comparisons between experiment and model simulation, (a) TufFoam35, and (b) PMDI20.

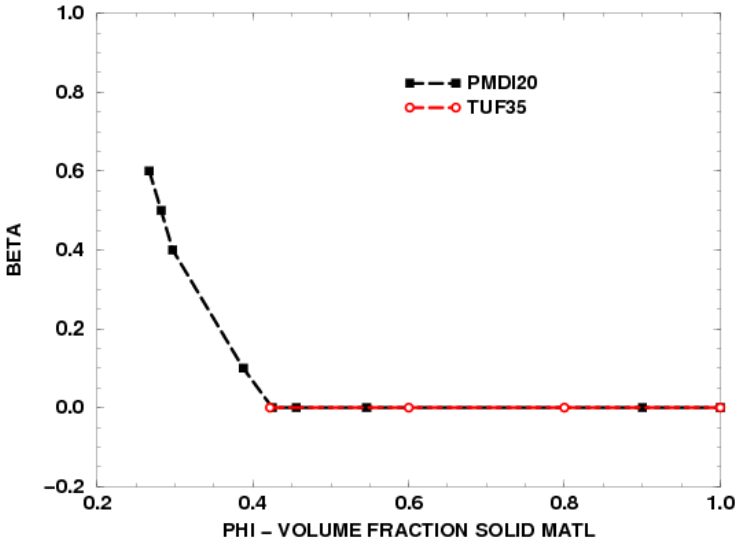

Figure 43 The value of parameter β.

4. TENSION

4.1. Experimental Method

4.1.1. Specimen

Figure 44(a) shows the design and dimensions of a plate dog-bone tensile specimen. The gage section is 1.0 inch long, 0.25 inch wide and 0.25 inch thickness. Load is applied at four curved surfaces by a pair of custom made fixtures, which has a matching radius of 0.75 inch. Figure 44(b) displays a specimen mounted in the loading fixtures. The installation is very easy, just dropping in.

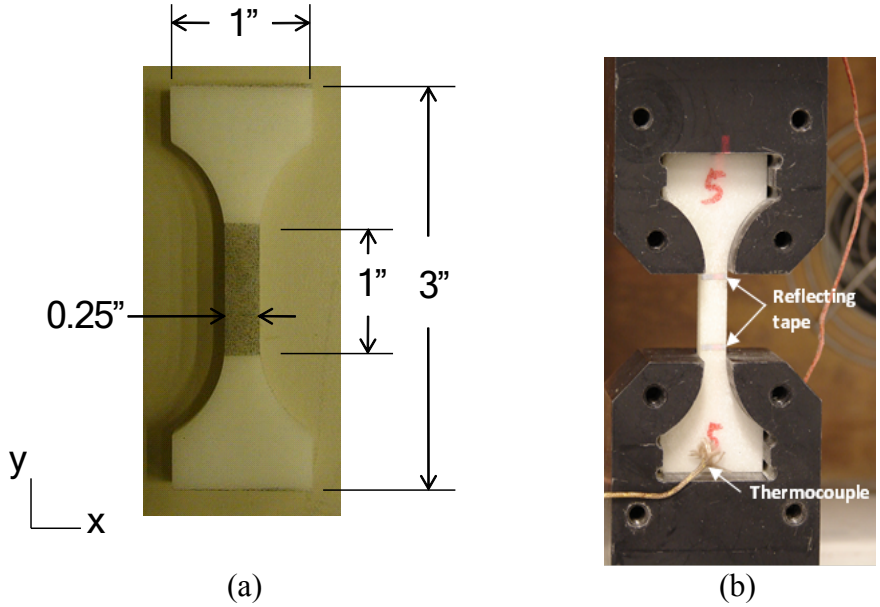

Figure 44 Foam tensile specimen.

4.1.2. Setup

The tensile experiments were completed in several modules, not all at once; so the setup might not be exactly the same each time. Generally, it was on the MTS bionic system due to its high precision displacement control and the convenience of hydraulic grips. The actuator is on the crosshead at the top and the system load cell is on the bottom. Figure 45 show two example setups that had been used. The self-aligned load train was always the same as illustrated in Fig. 45(a), from top: ball-and-socket joint, pull-rod, custom fixture, specimen, and symmetric for the bottom side. Some room temperature tests were conducted without an environmental chamber installed. Figure 45(b) shows a chamber is installed on the MTS frame.

Several strain measuring methods were utilized depending on the test condition and equipment availability. Laser extensometer was used most often. It requires two reflecting tapes to mark the gage section of the specimen as shown in Fig. 44 (b). Its scanning unit is mounted on the MTS frame with an adjustable arm, Fig. 45(b). Even with the environmental chamber closed,

the laser light works through the transparent window. Digital image analyses were used for strain measurement too, such as digital image correlation (DIC) or track eye motion analysis (TEMA) software. Sometimes a speckle pattern, Fig. 44(a), was applied for better results. The third method was clip-on mechanical extensometer, Fig. 46. It has the advantage of cold temperature testing, where the frost or fog makes the optical methods very challenging. All three methods have good strain resolution, 10^{-4}, for the test; mechanical extensometer has a slightly higher resolution.

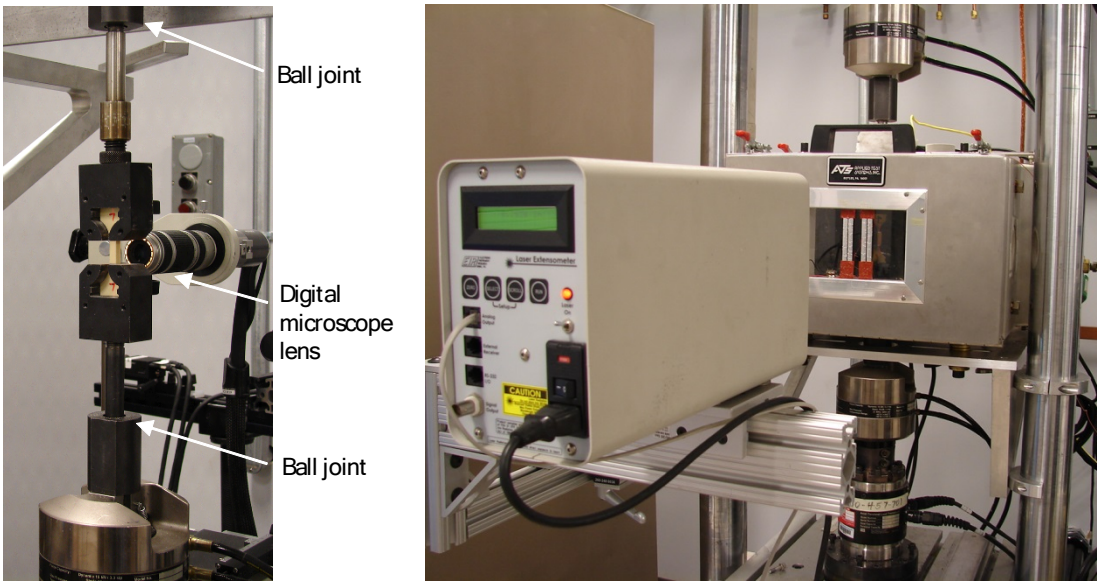

Figure 45 Foam tension experimental setup on MTS Bionic System, (a) without and (b) with an environmental chamber.

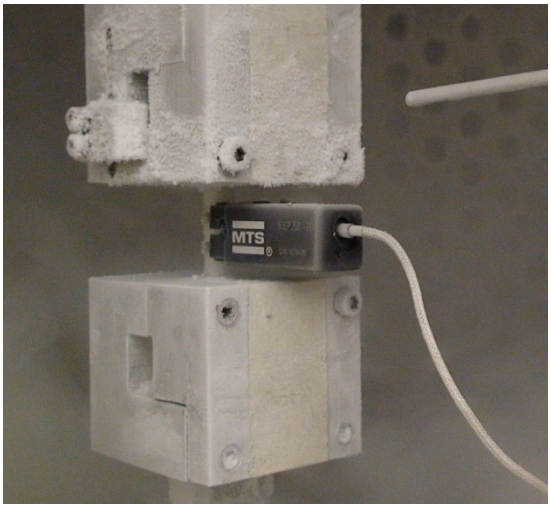

Figure 46 Using mechanical extensometer at cold temperatures.

4.2. Experiment and Results

4.2.1. PMDI foams

The test matrix of PMDI foam is listed in Table 13. The foam specimens were machined from the same billets as those used in the uniaxial compression. The tensile tests were all conducted at quasi-static rate, less than 10^{-3}/s, and only at two temperatures, 70 and 180^{o}F. The experimental results are plotted in Figs. 47 – 51.

Table 13 Quasi-static tension of PMDI foams

Specimen	Width (in)	Thickness (in)	Density (pcf)	Temperature (degree F)
PMDI10_2	0.252	0.254	8.57	70
PMDI10_3	0.254	0.252	8.64	70
PMDI10_4	0.253	0.261	8.25	180
PMDI10_5	0.251	0.279	8.48	70
PMDI10_6	0.253	0.253	8.61	180
PMDI10_7	0.252	0.260	7.92	70
PMDI20_1	0.255	0.250	24.52	70
PMDI20_2	0.255	0.252	18.69	70
PMDI20_3	0.254	0.258	24.40	70
PMDI20_4	0.255	0.267	18.61	180
PMDI20_5	0.254	0.255	19.12	180
PMDI20_7	0.255	0.261	18.59	70
PMDI30_1	0.255	0.251	27.15	70
PMDI30_2	0.256	0.254	26.93	70
PMDI30_3	0.254	0.237	26.66	70
PMDI30_4	0.255	0.260	27.31	180
PMDI30_5	0.254	0.248	27.67	180
PMDI40_1	0.254	0.258	35.96	70
PMDI40_2	0.255	0.262	36.13	70
PMDI40_4	0.254	0.257	35.91	180
PMDI40_5	0.256	0.228	39.24	180
PMDI50_1	0.254	0.258	49.53	70
PMDI50_2	0.254	0.257	50.09	70
PMDI50_3	0.254	0.217	55.73	70
PMDI50_4	0.254	0.234	54.31	180

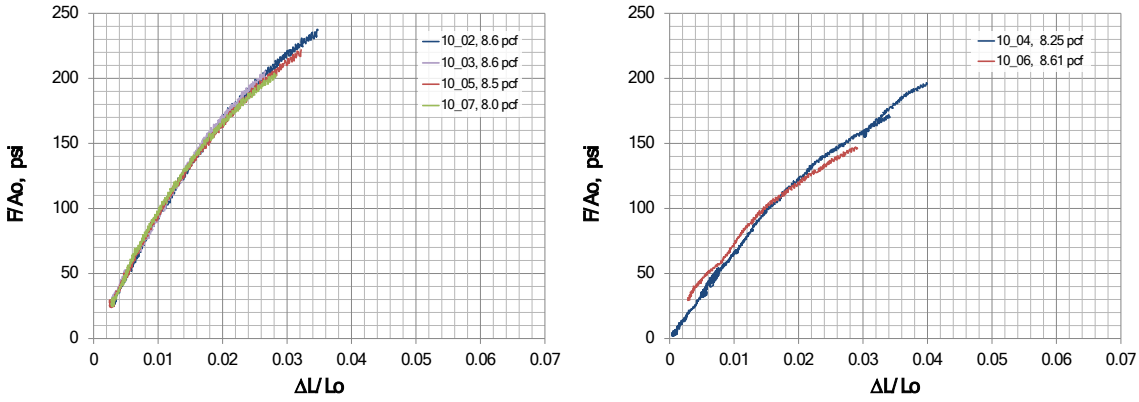

(a) (b)

Figure 47 Tensile stress-strain curves of PMDI10, (a) 70°F, and (b) 180°F.

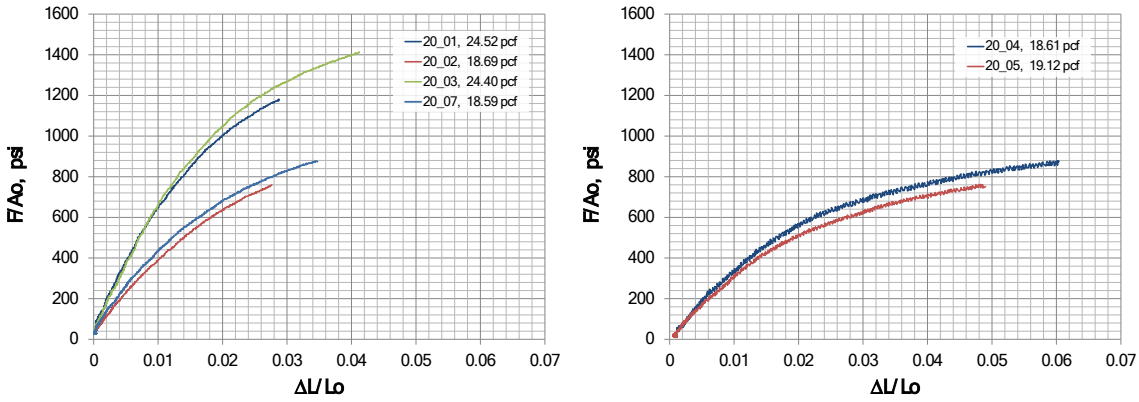

(a) (b)

Figure 48 Tensile stress-strain curves of PMDI20, (a) 70°F, and (b) 180°F.

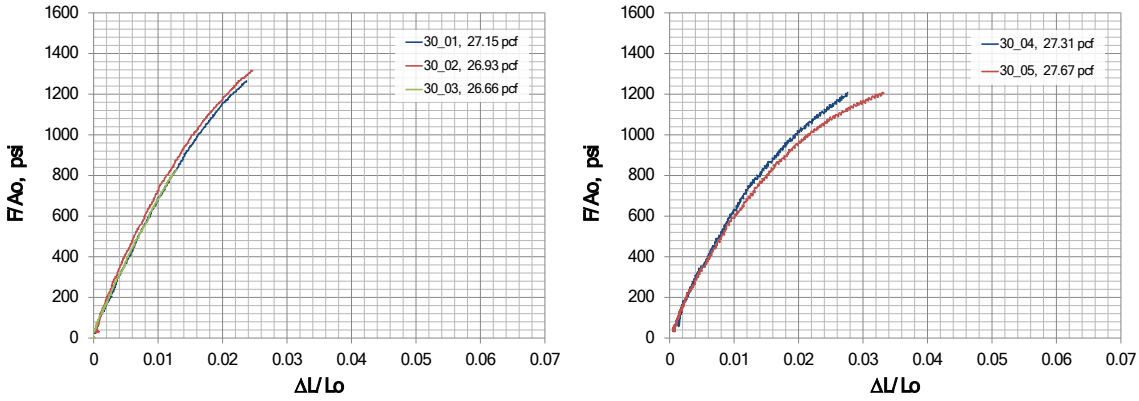

(a) (b)

Figure 49 Tensile stress-strain curves of PMDI30, (a) 70°F, and (b) 180°F.

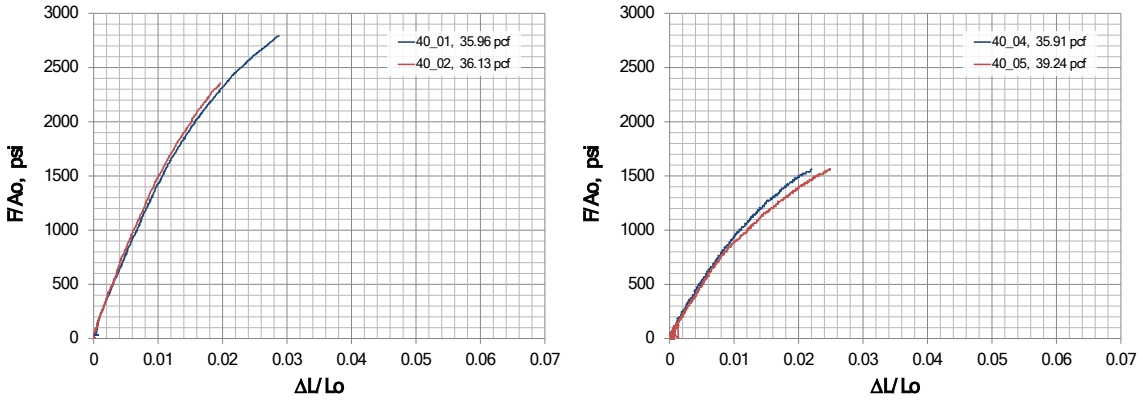

(a) (b)

Figure 50 Tensile stress-strain curves of PMDI40, (a) 70°F, and (b) 180°F.

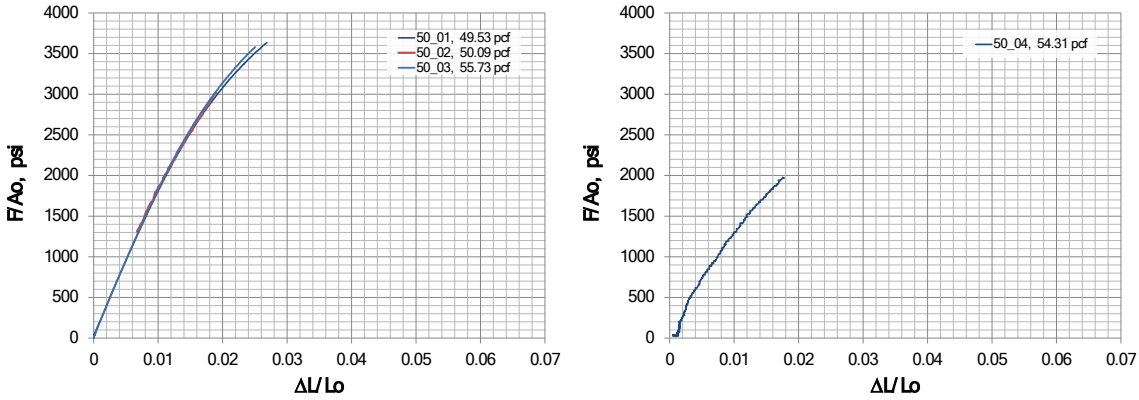

(a) (b)

Figure 51 Tensile stress-strain curves of PMDI50, (a) 70°F, and (b) 180°F.

4.2.2. PMDI20 Batch 2

Tensile tests were also performed on a different batch of PMDI20. The test conditions, listed in Table 14, included two strain rates, 0.001 and 1.0/s, and three temperatures, 70, -65, and 165 ^{o}F. The results are shown in Figs. 52 – 54. Two cases were similar to the previous set: 0.001/s at 70 and 165^{o}F. The room temperature result is comparable, but at 165 ^{o}F the failure stress is more than 20% lower than the previous test, 600 psi versus 800 psi.

4.2.3. TufFoam

Tensile tests of TufFoam35 and TufFoam65 are listed in Table 15. Stress-strain results are in Fig. 55 – 56. TufFoam appears to be more ductile than PMDI foams. The failure strain of TufFoan35 at room temperature almost doubles that of PMDI40. The high temperature deformation of TufFoam65 reaches more than 14% of strain.

Table 14 Tensile Tests of PMDI20 Batch 2

Specimen	Thickness (in)	Width (in)	Density (pcf)	Temperature (degree F)	Rate (s^{-1})
6	0.217	0.252	18.00	70	0.001
21	0.217	0.252	18.25	70	1.0
29	0.240	0.252	18.53	70	0.001
2	0.221	0.249	18.72	70	1.0
4	0.216	0.249	18.45	70	1.0
10	0.216	0.250	17.96	70	1.0
19	0.245	0.251	18.43	-65	0.001
23	0.215	0.254	18.14	-65	0.001
26	0.242	0.252	18.02	-65	0.001
1	0.244	0.249	19.49	-65	1.0
20	0.200	0.252	18.86	-65	1.0
22	0.220	0.253	17.77	-65	1.0
8	0.220	0.252	17.94	165	0.001
17	0.245	0.251	18.88	165	0.001
24	0.246	0.255	18.07	165	0.001
3	0.215	0.250	18.60	165	1.0
7	0.218	0.250	17.83	165	1.0
30	0.239	0.252	18.31	165	1.0

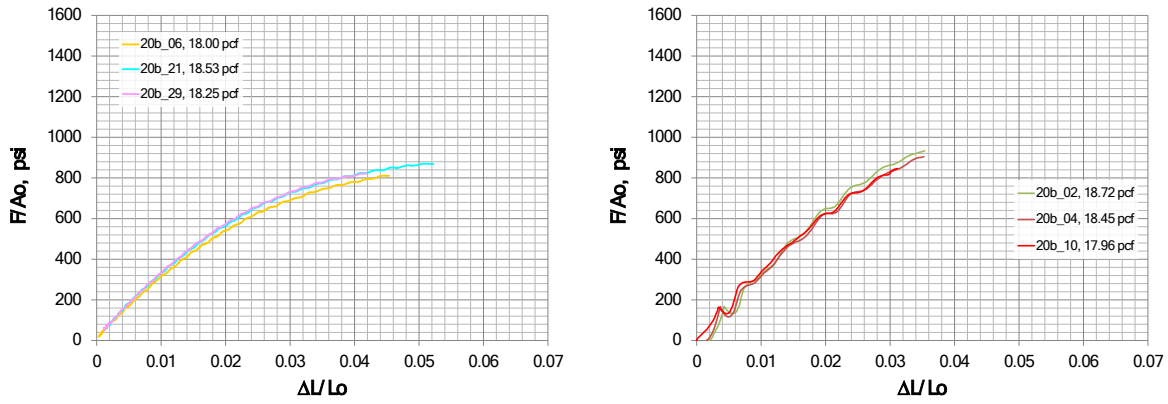

Figure 52 Tensile stress-strain curves of PMDI20 at 70°F, (a) 0.001/s, and (b) 1.0/s.

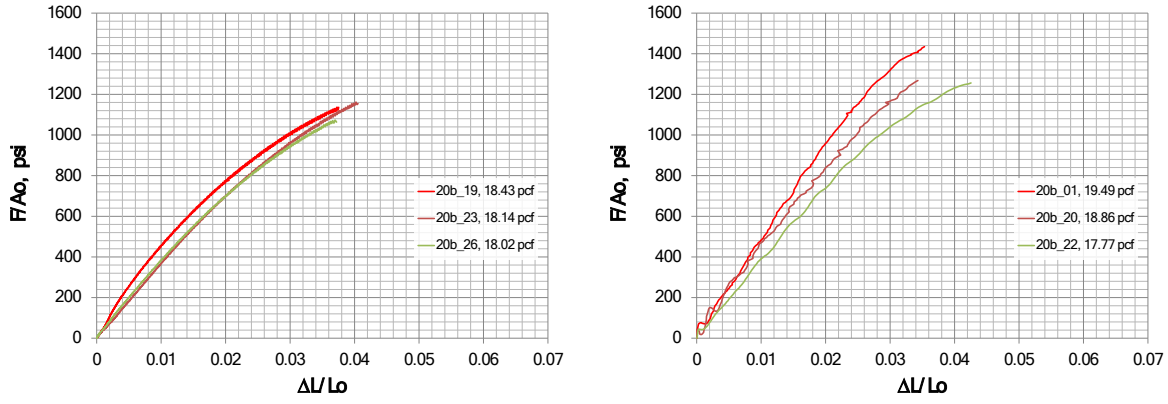

Figure 53 Tensile stress-strain curves of PMDI20 at -65°F, (a) 0.001/s, and (b) 1.0/s.

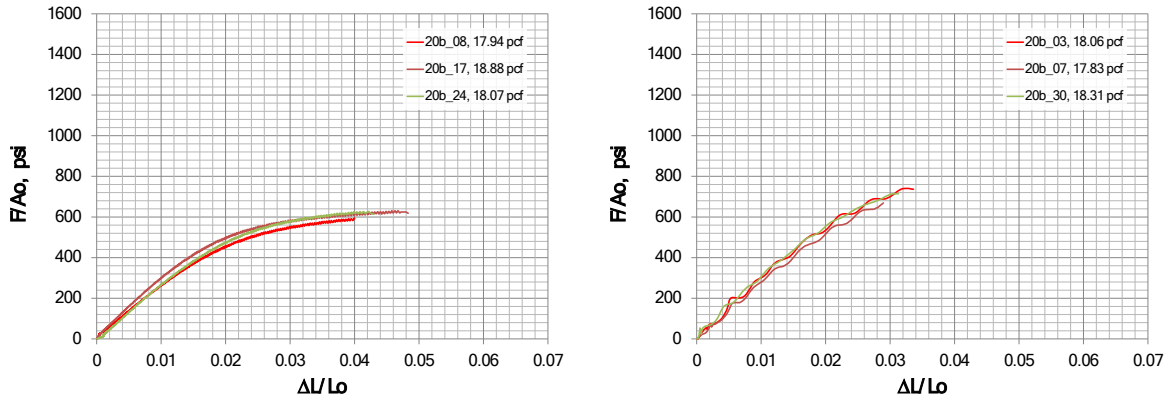

Figure 54 Tensile stress-strain curves of PMDI20 at 165°F, (a) 0.001/s, and (b) 1.0/s.

Table 15 Quasi-static tension of TufFoam

Specimen	Width (in)	Thickness (in)	Density (pcf)	Temperature (degree F)
Tuf35_1	0.256	0.233	38.50	70
Tuf35_2	0.254	0.252	34.47	70
Tuf35_3	0.255	0.217	38.39	70
Tuf35_4	0.254	0.255	34.90	180
Tuf35_5	0.256	0.264	34.96	180
Tuf35_6	0.255	0.259	35.27	70
Tuf65_2	0.250	0.250	59.73	70
Tuf65_3	0.250	0.248	58.59	70
Tuf65_5	0.250	0.250	59.73	180

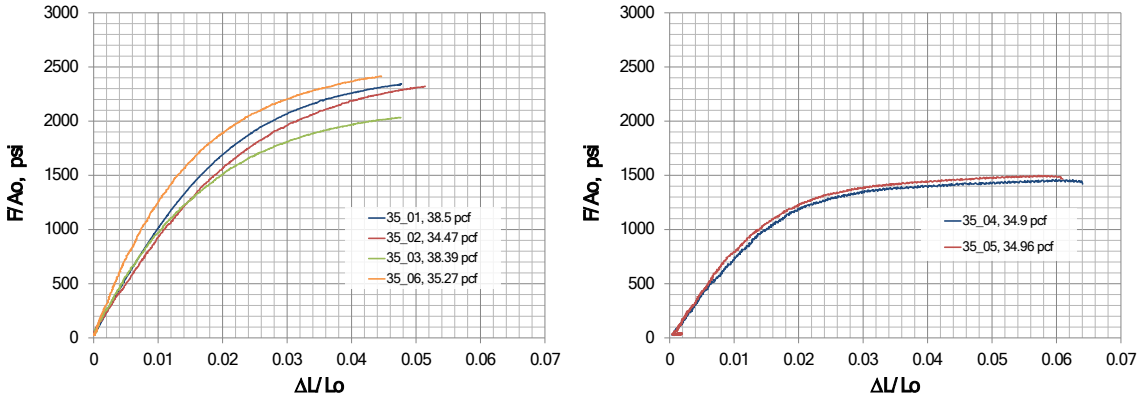

(a) (b)

Figure 55 Tensile stress-strain curves of TufFoam35, (a) 70°F, and (b) 180°F.

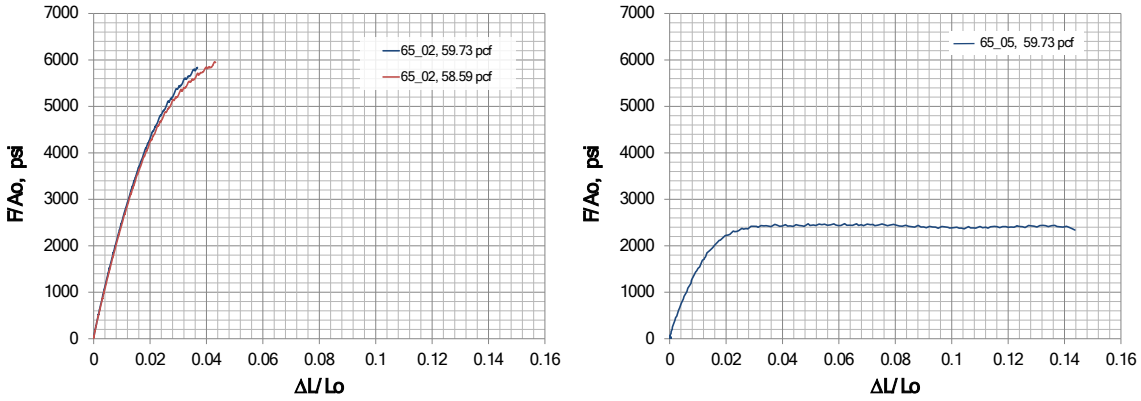

(a) (b)

Figure 56 Tensile stress-strain curves of TufFoam65, (a) 70°F, and (b) 180°F.

4.3. Effects of Density

For quasi-static tensile experiments, the tensile strength and initial tensile modulus are summarized in Figs. 57 and 58. Tensile and compressive moduli are comparable. Foam's tensile strength is generally lower than its compressive crush stress.

The effect of density on failure strain is not very clear, Fig. 59. Data is quite scattered. Ignoring the data of TufFoam65 at 180°F, it appears the failure strain decreases as the density increases.

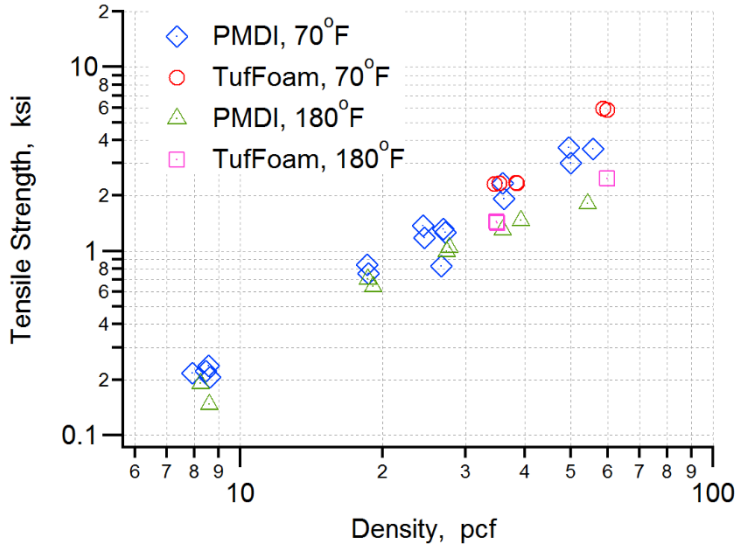

Figure 57 The density effect on tensile strength of foams.

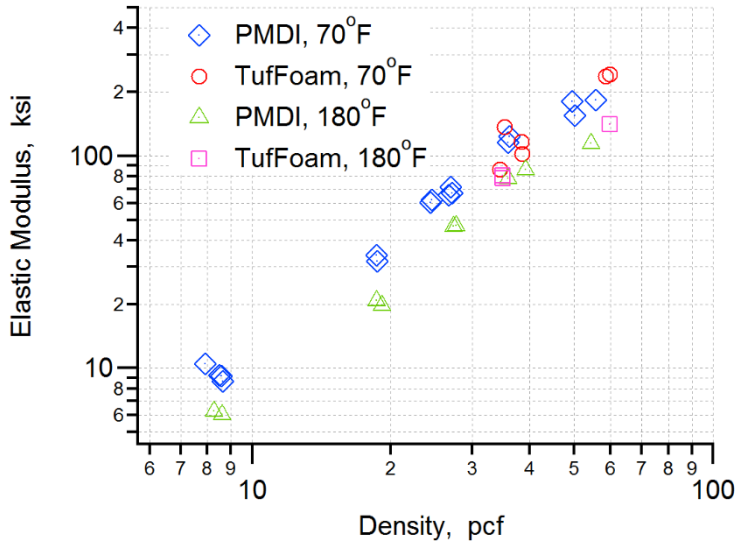

Figure 58 The density effect on tensile elastic modulus.

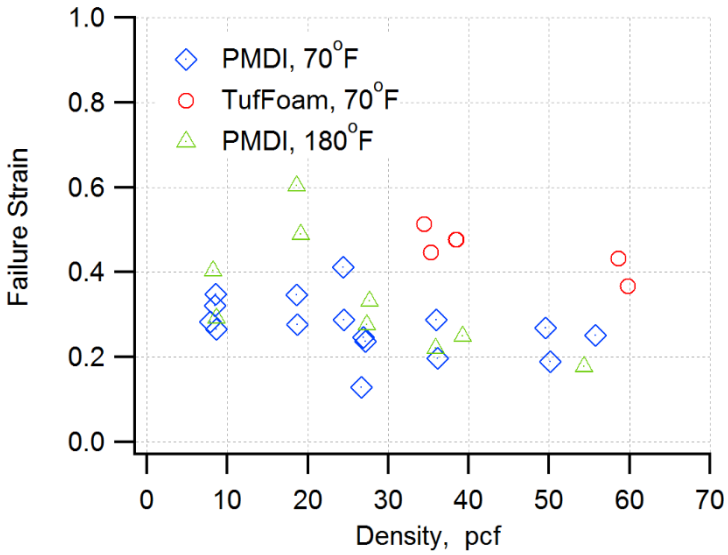

Figure 59 Tensile failure strain versus density.

5. BIAXIAL TENSION

Foam experiments described in above sections cover about two third of the shear-mean stress space, as shown in Fig. 60. On the right side of the uniaxial tension, there was basically no experimental data available about the yield and damage surfaces. Biaxial tension experiment was designed to probe the shape of those surfaces in that region.

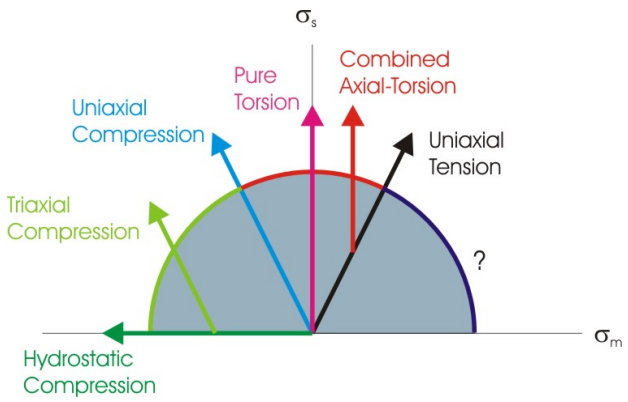

Figure 60 Loadings in shear-mean stress space.

5.1. Tube Tension and Pressurizing

The experiment utilized thin-wall type specimens. When a thin-wall tubular specimen is subjected to internal pressure *P* and tensile load *F* along its axis, Fig. 61, the tube wall experiences a uniform biaxial stress field with axial and hoop stresses σ_a and σ_h

$$F = A \cdot \sigma_a \quad \text{and} \quad P = \sigma_h \cdot (d_1 - d_2)/d_2 \tag{4}$$

where A is the cross-sectional area, d_1 and d_2 are outside and inside diameter of the tube, respectively.

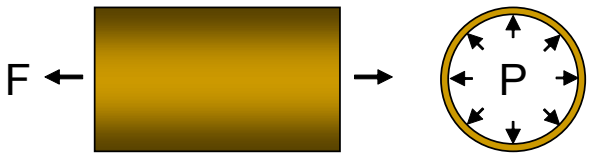

Figure 61 Axial loading and internal pressurizing of a thin wall cylinder.

5.2. Specimen Preparation

To prepare a foam tubular specimen for biaxial tension experiment, three steps were taken. The first step was to machine a foam tube, shown in Fig. 62(a). In this study PMDI20 was

considered. The nominal dimensions were: d_1 = 1.30 inch, d_2 = 1.03 inch, L = 5.5 inch. Since high pressure will break foam cell wall [2], a coating is necessary to protect the inner surface of the foam tube. So the second step was to coat the inside surface with GE Silicone RTV615. After many tries, the following process worked well. It involved mixing compounds, spreading the mixture on the inside surface, rotating the tube horizontally during curing at room temperature. The process was repeated for a second coating. The coated tube is shown in Fig. 62(b). The final thickness of the coating was about 0.06 inch. The last step was to attach the aluminum fixtures on both ends of the foam tube. Epoxy was applied on the aluminum-foam interface, and the specimen was assembled and cured on a custom-made alignment device. The finished specimen is shown in Fig. 62(c).

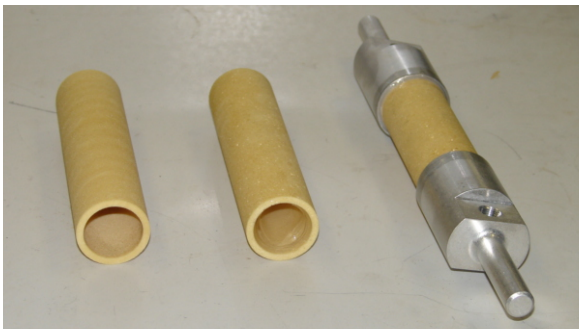

(a) (b) (c)

Figure 62 Three steps of preparing bi-axial tension specimens: (a) foam cylinder, (b) inside surface coating, and (c) fixture attachment.

5.2.1. Coating Material Characterization

With a layer of RTV coating, Fig. 63, Equation (4) becomes

$$F = \frac{\pi}{4}(d_1^{\,2} - d_2^{\,2})(\sigma_a)_{foam} + \frac{\pi}{4}(d_2^{\,2} - d_3^{\,2})(\sigma_a)_{RTV}$$

$$P = (\sigma_h)_{foam} \cdot \frac{d_1 - d_2}{d_3} + (\sigma_h)_{RTV} \cdot \frac{d_2 - d_3}{d_3} \qquad (5)$$

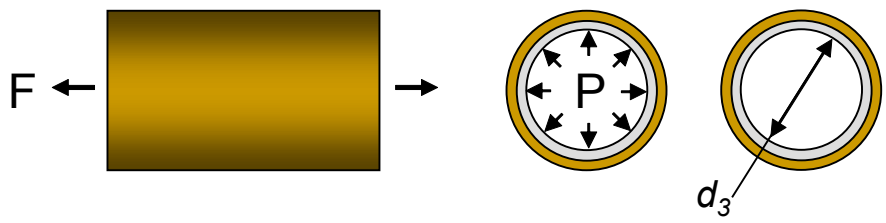

Figure 63 Axial loading and internal pressurizing of a thin wall cylinder with coating.

Since the strains of the foam and coating $(\varepsilon_i)_{foam}$ and $(\varepsilon_i)_{RTV}$, where i = a or h, are about the same; therefore, the stresses $(\sigma_i)_{foam}$ and $(\sigma_i)_{RTV}$ are approximately proportional to their elastic moduli. To evaluate the stresses of foams, the mechanical property of the coating material was needed.

A flat sheet of RTV615 was prepared. Dog-bone specimens were stamped out from the sheet for tensile tests, which were conducted on the Bionic system and the strain was measured by a laser extensometer. The test and result are shown in Fig. 64. The elastic modulus of the coating is $E_{RTV} \approx 140$ psi, which is much smaller than the modulus of PMDI20 $E_{foam} \approx 30{,}000$ psi. The stresses in the coating are much smaller than the stresses in the foam. The second term on the right side of Eq. (5) can be neglected, which make the evaluation of foam stresses rather straight forward.

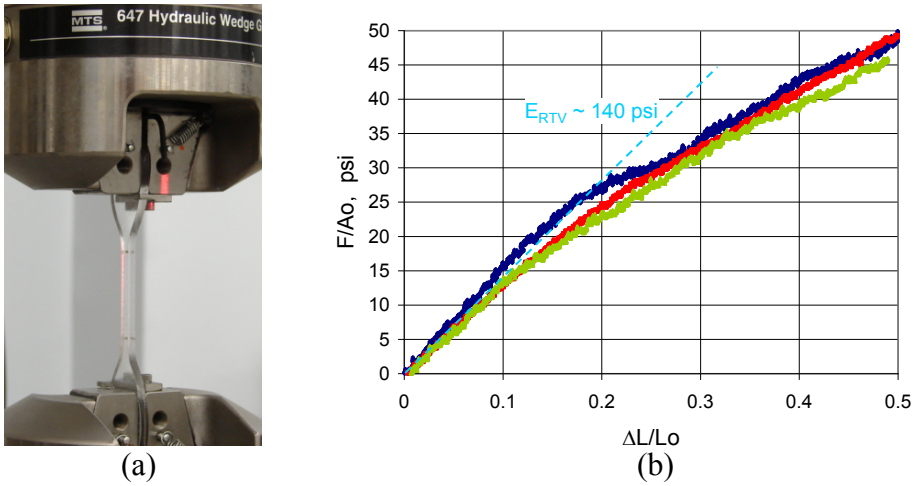

(a) (b)

Figure 64 Tensile test of RTV615, (a) experiment, and (b) stress-strain curves.

5.3. Experiment and Results

Biaxial experiment was setup on the Bionics (MTS858) system. It was modified to include a pressure channel. The water pressurizing unit is shown on the left side of Fig. 65(a). Figure 65(b) shows the close-up of a mounted specimen. A plastic pan was installed below the specimen to collect water when it broke. Axial and hoop strain were measured by laser and mechanical extensometers, respectively. All test were done by force and pressure control.

Six biaxial tension tests with proportional loading path were performed. The text matrix is tabulated in Table 16. Each path had a different σ_h / σ_a ratio. Actual stress paths are plotted in Fig. 66. All specimens were failed in brittle mode at the end of their path. Post-experiment specimens are displayed in Fig. 67. The color of the frame boarder matches the color of the path in Fig. 66. Most of the stress-strain curves of the major component of the test are plotted in Fig.

68. They are consistent with the result of dog bone tension, Fig. 48(a), but the strengths are lower.

Table 16 Test matrix and results of biaxial tension

Specimen	Density, pcf	σ_h/σ_a	$(\sigma_a)_{max}$, *psi*	$(\sigma_h)_{max}$, *psi*	$\sigma_{failure}$, *psi*
PMDI01	20.35	0.3	748	224	748
PMDI02	19.29	8.0	73	573	573
PMDI03	22.20	0.0	735	8	735
PMDI04	18.92	1.4	369	502	502
PMDI05	17.88	0.6	535	340	535
PMDI06	22.74	1.0	716	713	716

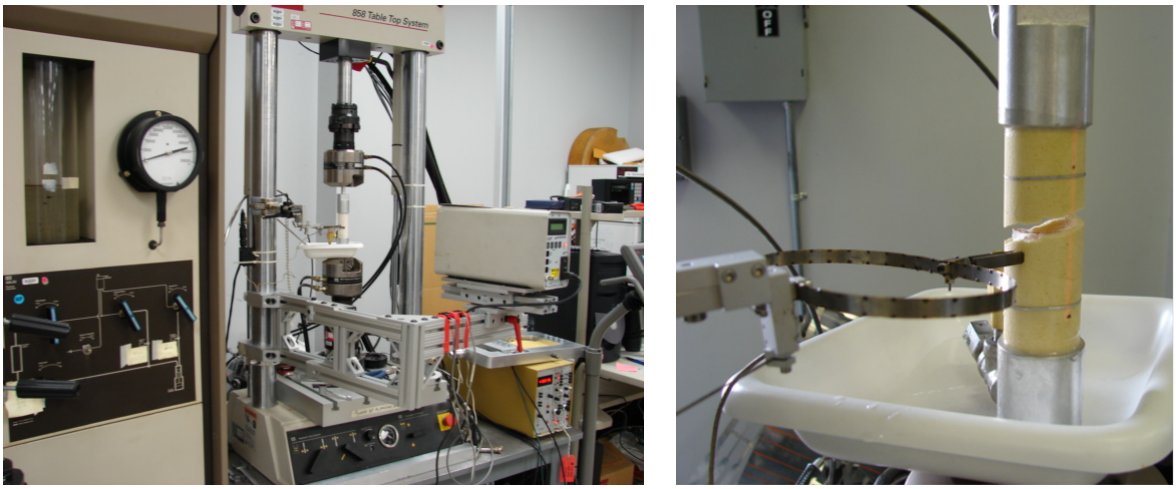

(a) (b)

Figure 65 Foam biaxial tension experiment, (a) setup, and (b) strain measurement.

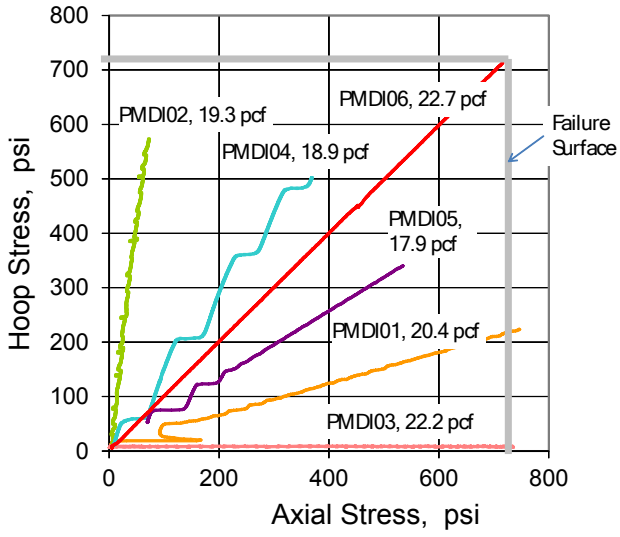

Figure 66 Biaxial loading paths in stress space.

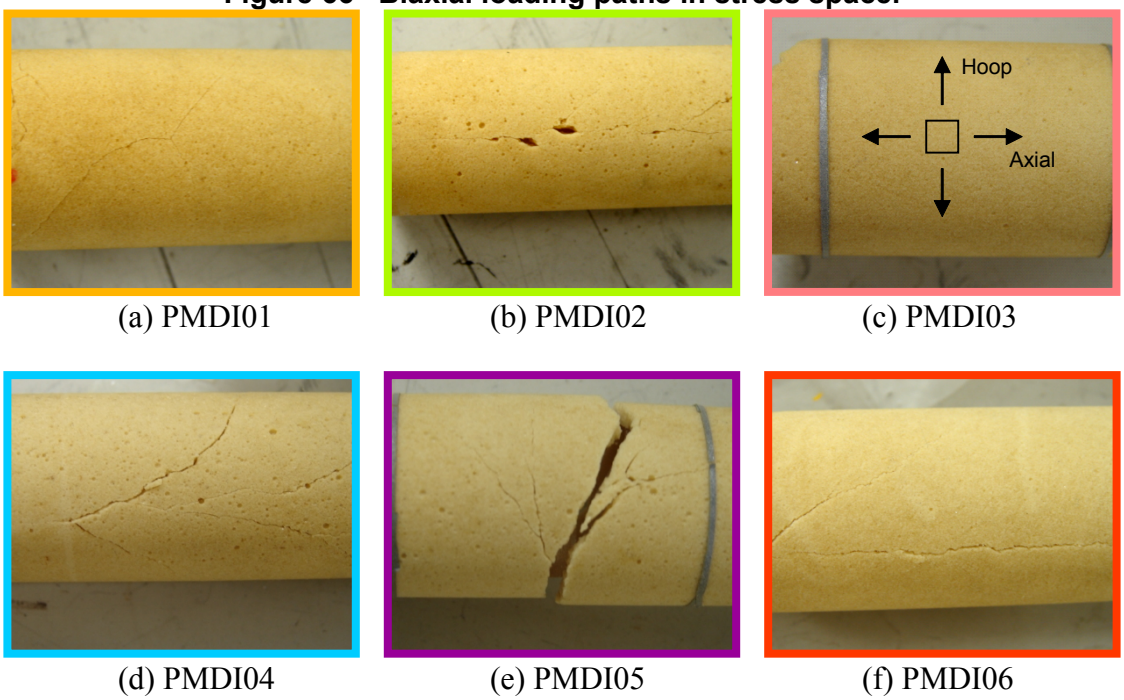

(a) PMDI01 (b) PMDI02 (c) PMDI03

(d) PMDI04 (e) PMDI05 (f) PMDI06

Figure 67 Post-experiment biaxial specimens.

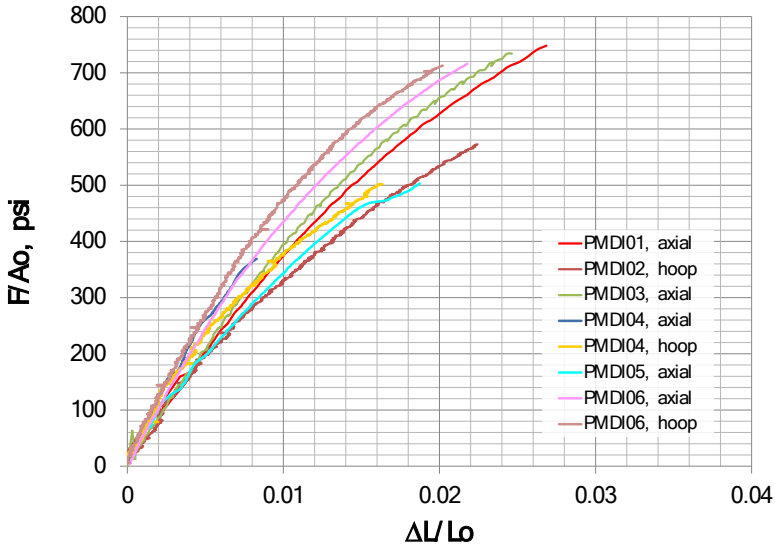

Figure 68 Stress-strain curves of PMDI20 biaxial tension experiments.

5.4. Discussion

The failure stresses of these specimens are also listed in Table x. For the loadings considered, σ_a and σ_h are principal stresses. The maximum principal stresses appear to cluster in two groups and do not have a consistent trend. Group 1, specimens PMDI01, PMDI03, and PMDI06, have the value $\sigma_1 = 730 \pm 15$ psi; the other three, Group 2, are $\sigma_1 = 537 \pm 35$ psi.

From the result of uniaxial tension, Fig. 57, the general trend observed is that the tensile failure stress is higher when the density is higher. The foam density varied from 17.9 to 22.7 pcf for specimens involved in the biaxial tension study. The specimens in Group 1 are the top three high densities specimens. It is reasonable that the Group 2 failure stresses are low.

Carefully examining the specimens, it is also noticeable that near the failure location (or cracks) Group 2 specimens clearly have voids, which cause pre-matured failure of a specimen. This can also see from the stress-strain plot, Fig. 68. For example, the modulus of PMDI02 is fairly lower than PMDI01 although their densities are quite close, which indicates damages (or voids) in PMDI02.

From initially undamaged specimens, Group I, principal stress failure criterion is a good approximation. The failure surface is shown as the thick gray line in Fig. 66.

6. SUMMARY

This report documented experiments that characterized foams mechanical behaviors. Two types of polyurethane foam were included, PMDI foam and TufFoam. Four major experiments were conducted: uniaxial compression, confined compression, uniaxial tension, and biaxial tension. The main experimental parameters considered in this study were density, temperature, and strain rate. They all have significant effects on foam's behavior. Quantitative data are presented. Other parameters such as specimen aspect ratio, lubrication, batch, etc. were also studied. Their influences, however, were rather minor.

Since the temperature and strain rate control as well as measurements of force, displacement and strain are well-established engineering methods, the uncertainties due to these variables should be very small, less than 1%; however, there are large scatters in crush stress, tensile strength, elastic modulus, etc. The major source of these scatter possibly comes from the foam material. The density could vary 25% for specimens machined from the same billet. In addition to density variations, void size and distribution also influence the results.

The data are mostly for foam models calibration, some are discovery, and some could be used for model validation.

7. REFERENCES

1. Michael Neilsen, Wei-Yang Lu, William Scherzinger, Terry Hinnerichs, David Lo, "Unified Creep Plasticity Damage (UCPD) Model for Rigid Polyurethane Foams," *to be published*.
2. Neilsen, M., Lu, W.-Y., Olsson, W., Hinnerichs, T., "A Viscoplastic Constitutive Model For Polyurethane Foams," IMECE2006-14551, Proceedings of IMECE, ASME Press.
3. Lu, W.-Y., Korellis, J., Lee, K., Grishaber, R., "Hydrostatic and uniaxial behavior of a high density polyurethane foam (FR-3720) at various temperatures," SAND93-8227, March 1993.
4. Zhang, J., Kikuchi, N., Li, V., Yee, A., and Nusholtz, G., "Constitutive Modeling Of Polymeric Foam Material Subjected To Dynamic Crash Loading," Int. J. Impact Engn 9 Vol. 21, No. 5, pp. 369 386. 1998.

Distribution (electronic copy)

Professor Weinong Chen
Purdue University
School of Aeronautics and Astronautics
701 W. Stadium Ave.
West Lafayette, IN 47907-2045
Email: wchen@purdue.edu

Professor Addis Kidane
University of South Carolina
Mechanical Engineering
300 Main Street
Columbia, SC 29208
Email: kidanea@cec.sc.edu

MS0346	Neilsen, Michael K.	01526
MS0346	Vangoethem, Douglas	01526
MS0382	Owen, Albert	02152
MS0382	Keil, Tyler	02153
MS0382	Levine, Ryan D.	02153
MS0382	Velasquez, Gabriel A.	02153
MS0557	Song, Bo	01558
MS0840	Fang, Huei Eliot.	01554
MS0840	Bean, James	01554
MS0840	Hinnerichs, Terry D.	01554
MS0840	Lo, Chi S.	01554
MS0840	Breivik, Nicole L.	01554
MS0840	Kmetyk, Lubomyra N.	01554
MS0840	Grange, Spencer	01554
MS0840	Hammetter, Chris	01554
MS1135	Epp, David	01531
MS9042	McIlroy, Andrew	08250
MS9042	Ostien, Jakob	08256
MS9042	Jin, Huiqing	08256
MS9042	Chiesa, Michael L.	08259
MS9042	Dike, Jay J.	08259
MS9106	Scheffel, Simon	08226
MS9403	Whinnery Jr., LeRoy L.	08223
MS9661	Korellis, John S.	082541
MS9957	Jin, Huiqing	08256
MS0899	Technical Library	09536


Sandia National Laboratories